Research Article

Motion of a Spot in a Reaction Diffusion System under the Influence of Chemotaxis

Satoshi Kawaguchi

Department of Complex and Intelligent Systems, School of Systems Information Science, Future University Hakodate, Hakodate 041-8655, Japan

Correspondence should be addressed to Satoshi Kawaguchi; satoshi@fun.ac.jp

We consider the motion of a spot under the influence of chemotaxis. We propose a two-component reaction diffusion system with a global coupling term and a Keller-Segel type chemotaxis term. For the system, we derive the equation of motion of the spot and the time evolution equation of the tensors. We show the existence of an upper limit for the velocity and a critical intensity for the chemotaxis, over which there is no circular motion. The chemotaxis suppresses the range of velocity for the circular motion. This braking effect on velocity originates from the refractory period behind the rear interface of the spot and the negative chemotactic velocity. The physical interpretation of the results and its plausibility are discussed.

1. Introduction

The behaviors of artificial and biological microswimmers such as oil droplets, bimetallic nanorods, catalytic Janus colloids, liposomes, flagellated bacteria, and *Volvox* have attracted widespread attention [1]. Under certain circumstances, some of these microswimmers are self-propelled particles, the mobility mechanism of which has been intensively studied [2, 3]. The motion of oil droplets, especially, has been studied in well-controlled experimental facilities with sufficient reproducibility. Although symmetric droplets cannot move in the absence of external force, the Marangoni effect can cause motion in the presence of an inhomogeneous chemical substance outside the droplet or a temperature gradient along the surface [4–6]. Numerical simulations and theoretical results support this mechanism and the existence of straight, circular, and complicated motions of droplets [7, 8], and experimental results qualitatively agree with the numerical results [9–12]. Droplet motion has also been the subject of a review article [13, 14].

In a two-dimensional reaction diffusion (RD) system, the droplet is often referred to as a spot solution. In order to systematically describe the motion of spots in an RD system, the time evolution equation of the spot was derived and the mechanism of elastic collision of moving spots was clarified in a previous study [15]. This study was extended by studies on the drift and rotation bifurcations of spot solutions in RD systems [16, 17]. In order to describe the deformations of the spot, tensors were introduced. The bifurcation diagram of the spot suggested that, with increasing velocity of the spot, rotation bifurcation occurred causing the straight motion to become destabilized into circular motion.

In addition to the Marangoni effect, which plays an important role in the motion of oil droplets, chemotaxis is an important property of cell migration; it is important in mass transfer and immunological response in biology. In inflammatory response, the neutrophils among blood cells have a remarkable migration potency (chemotaxis) and can change their form by generating pseudopods toward the antigen. In biophylaxis, several chemokines (chemoattractants) are released from the macrophages and mast cells. Then other immunocompetent cells (neutrophils) respond to the gradient of the chemoattractant. Consequently, the immunocompetent cells move unidirectionally to the source point of the antigen [18].

The mathematical model for chemotaxis was first proposed by Keller and Segel [19], wherein the gradient of the chemoattractant was taken into consideration for the flow of amoeba. Neutrophil migration was considered with a Keller-Segel type chemotaxis term in [20, 21]. In these studies, the Cahn-Hilliard (CH) equation was employed, and the kinematic properties and morphological changes of the crawling cell distribution were shown. In addition to the chemotaxis of the neutrophil, cancer cell invasion under haptotaxis was modeled by the CH equation [22, 23]. The haptotactic response of cancer cells is described by the gradient of the haptoattractant. However, in the above studies, the gradients of chemoattractant and haptoattractant are assumed to be constant; there is no feedback between the cells and these chemical substances.

As described above, with the recent increase in importance of chemotaxis in biology, medicine, and cytoengineering [24–27], many experimental and theoretical studies have been performed. Although there are model systems for the cell density and concentration of chemotactic substances, no mathematical analysis has been reported on the motion of the cell. Inspired by these points, we first propose an RD system including a naive Keller-Segel type chemotaxis term. The system is autonomous, the spot secretes a chemotactic substance, and the motion of the spot is influenced by it. For the proposed RD system, we apply the method reported in [16] to derive the equation of motion of the spot and time evolution equation of the tensors. Based on these equations, we study the bifurcation from straight motion to circular motion as well as the upper limit of the velocity of circular motion. In order to verify the theoretical result, we perform numerical simulations for the tensor model. The physical meaning and validity of the results are discussed.

2. Model Equation

We first consider the following three-component RD system with an activator u, a chemotactic substance v, and an inhibitor w:

$$\tau\epsilon\frac{\partial u}{\partial t} = \epsilon^2\nabla^2 u - \epsilon\nabla\cdot\left(u\nabla\chi\left(v\right)\right) \\ + H\left(u - p\left(w\right)\right) - u - v, \tag{1}$$

$$\frac{\partial v}{\partial t} = \nabla^2 v + u - \mu v, \tag{2}$$

$$T\frac{\partial w}{\partial t} = D\nabla^2 w + u + v - w - W, \tag{3}$$

where $p(w) = p_0 + \alpha w$, $p_0, \alpha, \tau, \epsilon, \mu, T, D$, and W are positive constants, and $H(z)$ is a step function satisfying $H = 0$ for $z < 0$ and $H = 1$ for $z > 0$. Throughout this study, we consider the system in a two-dimensional space, with $\nabla = (\partial_x, \partial_y)$ and $\epsilon \ll 1$. We choose μ such that the system is monostable. Here, we fix $\mu = 0.3$. In the above excitable system, there are two stationary states: a rest state and an excited state. The rest state is $(u, v, w) = (0, 0, -W)$, and the excited state has spatially nonuniform values of u, v, and w. Between the

rest and excited states, there appear boundary layers with thickness $O(\epsilon)$, connecting the two different states.

When the second term on the right hand side of (1) is absent, (1)–(3) describe an RD system with one activator and two inhibitors, which was studied in [28]. In that system, when τ is large, the localized domain (motionless spot solution) of an activator appears. With decreasing τ, the motionless spot is destabilized through static bifurcation or oscillatory bifurcation; however, when T is small and D and α are large, these bifurcations are suppressed by w. When τ is small, the motionless spot is primarily destabilized through translational bifurcation, causing the spot to move.

In the presence of the second term on the right hand side of (1), the moving spot is influenced by the chemotaxis. A system similar to that described by (1)–(3), but with bistability, was studied in [29]. In that system, the nonlinear term in (1) was replaced by $H(u - p(w)) - u$, and a front solution was obtained. Furthermore, maze patterns and branching from a front solution were observed. The stability analyses of the spot and front solutions were conducted by applying the singular perturbation method [30].

The time evolution equation for u is obtained using the conservation equation. The diffusion term is derived from $-\nabla \cdot \mathbf{J}$, where the flux $\mathbf{J}$ is the sum of the normal diffusion (random motility) term $\mathbf{J}_d$ and the chemotaxis term $\mathbf{J}_c$. That is, $\mathbf{J} = \mathbf{J}_d + \mathbf{J}_c$, where $\mathbf{J}_d = -\epsilon^2\nabla u$ and $\mathbf{J}_c = \epsilon u\nabla\chi(v)$. It should be noted that the signs of these fluxes are different. The sign of $\mathbf{J}_c$ suggests that the chemotaxis term provides a negative diffusion effect, which suppresses the expansion of u. The second term on the right hand side of (1) is the Keller-Segel type chemotaxis term; we express the chemotactic sensitivity function χ as $\chi(v) = k_c\chi_0(v)$, where $\chi_0(v) = f_0\theta v^2/(v^2 + \theta^2)$ with $\theta = 1.0$. In order to satisfy the condition $\max|d\chi_0/dv| = 1$, we choose $f_0 = 8\sqrt{3}/9$. We call k_c the intensity of chemotaxis [31].

In (3), T and D represent the relaxation time and diffusion constant of w, respectively. Let us consider a situation in which w plays the role of feedback to suppress the static bifurcation and oscillatory bifurcation. For the rapid feedback mechanism, T and D must be small and large, respectively. In the limits $T \to 0$ and $D \to \infty$, w becomes a time-dependent but spatially independent variable, which is denoted by $\langle w(t)\rangle$:

$$\langle w\left(t\right)\rangle = \frac{1}{\Omega_0}\int d\mathbf{r}w = \frac{1}{\Omega_0}\int d\mathbf{r}\left(u + v\right) - W, \tag{4}$$

where Ω_0 is the area of the entire system. Replacing w in $p(w)$ by $\langle w(t)\rangle$, $p(w)$ becomes a global coupling term. In the case where T is very small and D is very large, we reduce the three-component RD system to the following two-component RD system with a global coupling term:

$$\tau\epsilon\frac{\partial u}{\partial t} = \epsilon^2\nabla^2 u - \epsilon\nabla\cdot\left(u\nabla\chi\left(v\right)\right) + f\left\{u, v\right\} - v, \tag{5}$$

$$\frac{\partial v}{\partial t} = \nabla^2 v + u - \mu v, \tag{6}$$

where

$$f\{u, v\} = -u + H(u - p\{u, v\}). \qquad (7)$$

The functional $p\{u, v\}$ represents a global coupling term given by

$$p\{u, v\} = p_0 + \alpha\left[\int d\mathbf{r}(u + v) - W\right], \qquad (8)$$

where the integral is over the entire domain, and α and W are rescaled to absorb Ω_0: $\alpha' = \alpha/\Omega_0$ and $W' = W\Omega_0$, and the primes are dropped. α corresponds to the intensity of the global coupling, and the value of p_0 is chosen as $p_0 = 0.275$. Hereinafter, we consider the above two-component RD system to be described by (5) and (6).

In the absence of chemotaxis, (5) and (6) describe the same system proposed by Krischer and Mikhailov [32]. This system had an activator and an inhibitor, and, for large τ, the motionless spot (localized particle-like structure) in two dimensions was stable. With decreasing τ under a large α, it was shown that the system had a stable moving spot. In order to understand intuitively the bifurcation from the motionless spot to the moving spot, we consider the limit $\epsilon \to 0$. In the limit $\epsilon \to 0$, the boundary layer of u becomes an interface, as shown in Figure 1. The location of the interface is defined by the condition $u(\mathbf{r}, t) = p$. In this limit, u and v satisfy the relation $(u + v) = 1$ (inside the domain) and 0 (outside the domain), which is obtained from (5). In the limits of $\alpha \to \infty$ and $\epsilon \to 0$, the area of the spot is conserved; using (8), we obtain

$$\int d\mathbf{r}(u + v) = W. \qquad (9)$$

This restriction prohibits the expansion and oscillation of the spot; the translational bifurcation firstly occurs with decreasing τ. Even for finite values of a large α and small ϵ, the area of the spot is approximately conserved by the feedback mechanism. This supports the existence of a moving spot for small τ with large α. In contrast, for small α, the static bifurcation or oscillatory bifurcation firstly occurs with decreasing τ, and the motionless spot is destabilized to form an expanding wave or is disintegrated by unstable oscillation.

Although the bifurcation from a motionless spot to a straight moving spot and the collision of two moving spots were studied in [32], other types of moving spot were not studied. Recently, the bifurcation of the spot from straight motion to circular motion was theoretically analyzed for the system described by (5) and (6) without the chemotaxis term [16]. The result suggested that there was a critical value τ_c for the bifurcation of stationary straight motion. Although the straight motion was stable for $\tau > \tau_c$, it was destabilized by rotation (straight-circular-motion) bifurcation for $\tau \leq \tau_c$. In other words, the straight motion was destabilized into circular motion with increasing velocity.

In this study, we assume that the localized domain (spot) of an activator exists under global feedback in the system described by (5) and (6). In the system, the chemotactic substance is secreted from inside the spot, and the motion of the spot is influenced by the chemotaxis. In order to study the
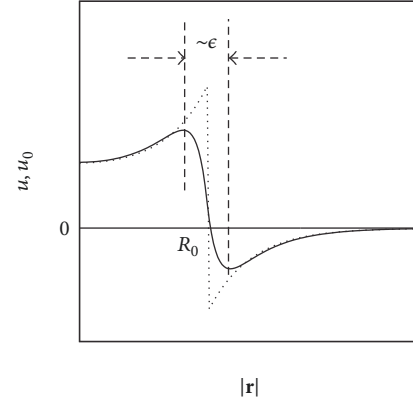

FIGURE 1: Boundary layer and interface. The solid and dotted curves correspond to $u(\mathbf{r}, t)$ and $u_0(\mathbf{r}, t) = \lim_{\epsilon \to 0} u(\mathbf{r}, t)$ along a radial direction, respectively, that is, $u(|\mathbf{r}|, t)$ and $u_0(|\mathbf{r}|, t)$. In the finite ϵ, $u(|\mathbf{r}|, t)$ has a boundary layer around $|\mathbf{r}| \sim R_0$ with the thickness of ϵ, where R_0 is determined by the condition $u(|\mathbf{r}| = R_0) = p$. $u_0(|\mathbf{r}|, t)$ does not have a boundary layer but has a sharp interface at $|\mathbf{r}| = R_0$.

influence of chemotaxis on the motion of a spot, we apply the technique reported in [16] to the system described by (5) and (6). For this purpose, we first derive the radially symmetric equilibrium solution of (5) and (6) in the limit $\epsilon \to 0$. In this limit, (6) becomes

$$\frac{\partial v}{\partial t} = \nabla^2 v + H(u - p) - \beta v, \qquad (10)$$

where $\beta = 1 + \mu$. Setting $\partial v/\partial t = 0$ in (10), (10) becomes

$$\left(\frac{d^2}{dr^2} + \frac{1}{r}\frac{d}{dr}\right)v - \beta v + H(R_0 - r) = 0, \qquad (11)$$

where $r = |\mathbf{r}|$ and R_0 is the equilibrium radius of the symmetric spot. We impose the boundary conditions on $v(r)$ as

$$\frac{dv(0)}{dr} = 0,$$
$$v(R_0+) = v(R_0-),$$
$$\frac{dv(R_0+)}{dr} = \frac{dv(R_0-)}{dr}, \qquad (12)$$
$$v(\infty) = 0.$$

The radially symmetric equilibrium solution of (10) in two dimensions is given by

$$\bar{v}(r)$$
$$= \begin{cases} \dfrac{1}{\beta} - \dfrac{R_0}{\sqrt{\beta}}K_1\left(\sqrt{\beta}R_0\right)I_0\left(\sqrt{\beta}r\right), & 0 < r < R_0, \\ \dfrac{R_0}{\sqrt{\beta}}I_1\left(\sqrt{\beta}R_0\right)K_0\left(\sqrt{\beta}r\right), & R_0 < r < \infty, \end{cases} \qquad (13)$$

where I_n and K_n are the modified Bessel functions of the first and second kinds of order n, respectively. The corresponding

solution of $u(r)$ is given by $\overline{u}(r) = H(R_0 - r) - \overline{v}(r)$. The above equilibrium solution is employed to study the motion of the spot in the following sections.

3. Equation of Motion of the Interface

As ϵ is small, the width of the boundary layer is small, and, therefore, the value of u changes sharply while that of v changes smoothly around the boundary layer. The velocity of the flat interface is a function of the value of v on the interface. In order to consider the dynamics of the spot in the system, we derive the equation of motion of the interface. The time evolution equation of the interface is described [16, 30, 33] by

$$\tau V = \tau C(h) + \epsilon \kappa + L, \tag{14}$$

where $C(h)$ is the velocity of a flat interface; κ is the curvature of the interface, the sign of which is chosen such that it is positive when the center of the curvature is outside of the excited domain; and h is the value of v on the interface. V is the normal component of the velocity, and L is the Lagrange multiplier for the constraint of domain area conservation (9). For the moving spot, this condition corresponds to

$$\int d\omega V(\omega) = 0, \tag{15}$$

where $d\omega$ is the infinitesimal length of the interface and the integral is carried over the entire interface.

We first consider the velocity of the interface in one dimension in (5) and (6). With the detailed derivations given in Appendix A, the velocity $\tau C(h)$ is obtained as

$$\tau C(h) = \frac{2(1/2 - h - p)}{[(h+p)(1-h-p)]^{1/2}}$$
$$+ \left(\frac{d\chi}{dv}\right)\Big|_i \left(\frac{dv}{dx}\right)\Big|_i, \tag{16}$$

where p is a global coupling term (8). $\tau C(h)$ consists of two components: the velocity of the traveling front solution in one dimension and the chemotactic velocity.

In two dimensions, the velocity of a flat interface directed along $\mathbf{n}$ is given by

$$\tau C(h) = \frac{2(1/2 - h - p)}{[(h+p)(1-h-p)]^{1/2}} + k_c \chi_0'(v) \left(\frac{dv}{d\mathbf{n}}\right)\Big|_i \tag{17}$$
$$\equiv P(h) + Q(h)(\mathbf{n} \cdot \nabla) v|_i,$$

where $\chi_0'(v) = d\chi_0(v)/dv$ and $A|_i$ represents the value of function A evaluated on the interface. $\mathbf{n}$ is a unit normal vector on the interface, and $(dv/d\mathbf{n})$ is a normal derivative.

When the motion of the interface of the spot is slow compared with the relaxation rate of the chemotactic substance, the left hand side of (10), $(\partial v/\partial t)$, is small. In this case, we deal with the time derivative of v in (10) as a perturbation.

The asymptotic solution of (10) is written by perturbation expansion using the Green function G as

$$v(\mathbf{r}, t) = GH - GG\frac{\partial H}{\partial t} + GGG\frac{\partial^2 H}{\partial t^2} - GGGG\frac{\partial^3 H}{\partial t^3} \tag{18}$$
$$+ \cdots,$$

where G is Green's function satisfying the equation

$$(\nabla^2 - \beta) G(\mathbf{r} - \mathbf{r}') = -\delta(\mathbf{r} - \mathbf{r}'). \tag{19}$$

In (18), GH represents the integral

$$GH = \int d\mathbf{r}_1 G(\mathbf{r} - \mathbf{r}_1) H(\mathbf{r}_1, t),$$
$$GG\frac{\partial H}{\partial t} = \int d\mathbf{r}_1 d\mathbf{r}_2 G(\mathbf{r} - \mathbf{r}_1) G(\mathbf{r}_1 - \mathbf{r}_2) \frac{\partial H(\mathbf{r}_2, t)}{\partial t}, \tag{20}$$
$$\cdots = \cdots,$$

for brevity. In this study, we consider the situation in which the motionless spot is destabilized supercritically and the spot moves with an arbitrarily small velocity. Then, we can safely apply the perturbative expansion of v in terms of G as in (18).

4. Deformed Spot Dynamics

In this section, we derive the equation of motion of the spot. In order to describe the deformations of the spot, tensors are introduced. The tensors depend on time, and the time evolution equation of the tensors are derived following [16].

4.1. Description of Deformed Spot. We firstly describe the position and velocity of a deformed spot. The motion of the spot consists of two components: the motion of the center of gravity and the motion of the interface relative to the center of gravity. The center of gravity is denoted by $\boldsymbol{\rho}$, and the velocity of the center of gravity is given by

$$\frac{d\boldsymbol{\rho}}{dt} = \frac{1}{\Omega} \int d\omega V(\omega) \mathbf{R}(\omega) \equiv \mathbf{v}, \tag{21}$$

where Ω is the area of the spot and $\mathbf{R}(\omega)$ is a position vector measured from the center of gravity. We consider the case that $\mathbf{R}(\omega)$ is a single valued function of ϕ_r, which is given as

$$\mathbf{R}(\omega) = R(\phi_r) \mathbf{e}_r, \tag{22}$$

where $\mathbf{e}_r$ is a radial unit vector and $R(\phi_r)$ is the distance between the center of gravity and a point on the interface, which is directed to an angle ϕ_r with respect to the x axis. Using the definition of $\mathbf{R}(\omega)$, $d\omega$ is given by

$$d\omega = \left|\frac{d\mathbf{R}}{d\phi_r}\right| d\phi_r = \sqrt{R^2 + R'^2} d\phi_r, \tag{23}$$

where $R' = dR(\phi_r)/d\phi_r$. For the deformed spot, the radius is given by

$$R(\phi_r) = R_0 + \delta R(\phi_r, t) \tag{24}$$

with

$$\delta R\left(\phi_r, t\right) = \sum_{n=-\infty}^{\infty} c_n\left(t\right) e^{in\phi_r}, \tag{25}$$

where $i = \sqrt{-1}$, R_0 is the equilibrium radius of the symmetric spot, and δR corresponds to the deviation. In the expansion of δR, $c_{\pm n}$ corresponds to a $(2\pi/n)$-periodic deformation. According to the area conservation equation (9), $c_0 = 0$. In addition, we exclude the terms of $n = \pm 1$ because the translational motion of the spot is incorporated in $\boldsymbol{\rho}$. Thus, we set $c_{\pm 1} = 0$. Using (24), the curvature κ and the normal component of the velocity V are given up to the first order of the deviations as

$$\kappa\left(\phi_r, t\right) = -\frac{1}{R_0} - \frac{1}{R_0^2} \sum_{n=-\infty}^{\infty} \left(n^2 - 1\right) c_n\left(t\right) e^{in\phi_r}, \tag{26}$$

$$V\left(\phi_r, t\right) = \mathbf{v} \cdot \mathbf{n} + \sum_{n=-\infty}^{\infty} \dot{c}_n\left(t\right) e^{in\phi_r}, \tag{27}$$

respectively, where the overdot denotes the time derivative.

For a general function $A(\mathbf{r}, t)$, the Fourier transformation and its reverse transformation in two dimensions are defined as

$$A_{\mathbf{q}}\left(t\right) = \int d\mathbf{r} A\left(\mathbf{r}, t\right) e^{-i\mathbf{q}\cdot\mathbf{r}}, \tag{28}$$

$$A\left(\mathbf{r}, t\right) = \frac{1}{(2\pi)^2} \int d\mathbf{q} A_{\mathbf{q}}\left(t\right) e^{i\mathbf{q}\cdot\mathbf{r}} \equiv \int_{\mathbf{q}} A_{\mathbf{q}}\left(t\right) e^{i\mathbf{q}\cdot\mathbf{r}}, \tag{29}$$

respectively, where $\int_{\mathbf{q}} = \int d\mathbf{q}/(2\pi)^2$ for brevity. For an isolated domain that forms a single loop without crossing, the step function $H(u - p) = H(R - |\mathbf{r} - \boldsymbol{\rho}|)$ is transformed by the Fourier transformation as

$$H_{\mathbf{q}} = \int d\mathbf{r} H\left(u - p\right) e^{-i\mathbf{q}\cdot\mathbf{r}} = \int_{|\mathbf{r}-\boldsymbol{\rho}|<R} d\mathbf{r} e^{-i\mathbf{q}\cdot\mathbf{r}}. \tag{30}$$

Substituting (24) into (30), we obtain the expansion of $H_{\mathbf{q}}$ up to the first order of δR as

$$H_{\mathbf{q}} = H_{\mathbf{q}}^{(0)} + H_{\mathbf{q}}^{(1)},$$

$$H_{\mathbf{q}}^{(0)} = \frac{2\pi R_0}{q} J_1\left(qR_0\right), \tag{31}$$

$$H_{\mathbf{q}}^{(1)} = 2\pi R_0 \sum_n c_n\left(t\right) i^{-n} e^{in\phi_q} J_n\left(qR_0\right),$$

where $q = |\mathbf{q}|$, ϕ_q is the angle between $\mathbf{q}$ and the x-axis, and J_n is a Bessel function of the first kind of order n.

4.2. Equation of Motion of a Spot.

We derive the equation of motion of a spot from (14). τC is given as functions of h and $\widetilde{h}$ by (17), in which we used the notation $\widetilde{h} = (dv/d\mathbf{n})|_i = (\mathbf{n} \cdot \nabla)v|_i$. When the velocity of the spot is small, the deformation of the circle is small. For this situation, we derive the deviations of h and $\widetilde{h}$ from their stationary values

as a power series of τC. Using (18), we first expand h and $\widetilde{h}$ up to the fourth-order time derivatives as

$$h = h_0 + h_1 + h_2 + h_3 + h_4, \tag{32}$$

$$\widetilde{h} = \widetilde{h}_0 + \widetilde{h}_1 + \widetilde{h}_2 + \widetilde{h}_3 + \widetilde{h}_4, \tag{33}$$

respectively, where

$$h_0 = \int_{\mathbf{q}} G_q H_{\mathbf{q}} e^{i\mathbf{q}\cdot\mathbf{R}(\omega)},$$

$$h_1 = h_{1,1} + h_{1,2}$$

$$= i \int_{\mathbf{q}} (\mathbf{v}\cdot\mathbf{q}) G_q^2 H_{\mathbf{q}} e^{i\mathbf{q}\cdot\mathbf{R}(\omega)} - \int_{\mathbf{q}} G_q^2 \left(\frac{\partial H_{\mathbf{q}}}{\partial t}\right) e^{i\mathbf{q}\cdot\mathbf{R}(\omega)},$$

$$h_2 = h_{2,1} + h_{2,2} + h_{2,3}$$

$$= -i \int_{\mathbf{q}} (\dot{\mathbf{v}}\cdot\mathbf{q}) G_q^3 H_{\mathbf{q}} e^{i\mathbf{q}\cdot\mathbf{R}(\omega)}$$

$$- \int_{\mathbf{q}} (\mathbf{v}\cdot\mathbf{q})^2 G_q^3 H_{\mathbf{q}} e^{i\mathbf{q}\cdot\mathbf{R}(\omega)}$$

$$+ \int_{\mathbf{q}} G_q^3 \left(\frac{\partial^2 H_{\mathbf{q}}}{\partial t^2}\right) e^{i\mathbf{q}\cdot\mathbf{R}(\omega)},$$

$$h_3 = -i \int_{\mathbf{q}} (\mathbf{v}\cdot\mathbf{q})^3 G_q^4 H_{\mathbf{q}} e^{i\mathbf{q}\cdot\mathbf{R}(\omega)},$$

$$h_4 = \int_{\mathbf{q}} (\mathbf{v}\cdot\mathbf{q})^4 G_q^5 H_{\mathbf{q}} e^{i\mathbf{q}\cdot\mathbf{R}(\omega)},$$

$$\widetilde{h}_0 = i \int_{\mathbf{q}} (\mathbf{n}\cdot\mathbf{q}) G_q H_{\mathbf{q}} e^{i\mathbf{q}\cdot\mathbf{R}(\omega)},$$

$$\widetilde{h}_1 = \widetilde{h}_{1,1} + \widetilde{h}_{1,2}$$

$$= -\int_{\mathbf{q}} (\mathbf{n}\cdot\mathbf{q})(\mathbf{v}\cdot\mathbf{q}) G_q^2 H_{\mathbf{q}} e^{i\mathbf{q}\cdot\mathbf{R}(\omega)}$$

$$- i \int_{\mathbf{q}} (\mathbf{n}\cdot\mathbf{q}) G_q^2 \left(\frac{\partial H_{\mathbf{q}}}{\partial t}\right) e^{i\mathbf{q}\cdot\mathbf{R}(\omega)},$$

$$\widetilde{h}_2 = \widetilde{h}_{2,1} + \widetilde{h}_{2,2} + \widetilde{h}_{2,3}$$

$$= \int_{\mathbf{q}} (\mathbf{n}\cdot\mathbf{q})(\dot{\mathbf{v}}\cdot\mathbf{q}) G_q^3 H_{\mathbf{q}} e^{i\mathbf{q}\cdot\mathbf{R}(\omega)}$$

$$- i \int_{\mathbf{q}} (\mathbf{n}\cdot\mathbf{q})(\mathbf{v}\cdot\mathbf{q})^2 G_q^3 H_{\mathbf{q}} e^{i\mathbf{q}\cdot\mathbf{R}(\omega)}$$

$$+ i \int_{\mathbf{q}} (\mathbf{n}\cdot\mathbf{q}) G_q^3 \left(\frac{\partial^2 H_{\mathbf{q}}}{\partial t^2}\right) e^{i\mathbf{q}\cdot\mathbf{R}(\omega)},$$

$$\widetilde{h}_3 = \int_{\mathbf{q}} (\mathbf{n}\cdot\mathbf{q})(\mathbf{v}\cdot\mathbf{q})^3 G_q^4 H_{\mathbf{q}} e^{i\mathbf{q}\cdot\mathbf{R}(\omega)},$$

$$\widetilde{h}_4 = i \int_{\mathbf{q}} (\mathbf{n}\cdot\mathbf{q})(\mathbf{v}\cdot\mathbf{q})^4 G_q^5 H_{\mathbf{q}} e^{i\mathbf{q}\cdot\mathbf{R}(\omega)}$$
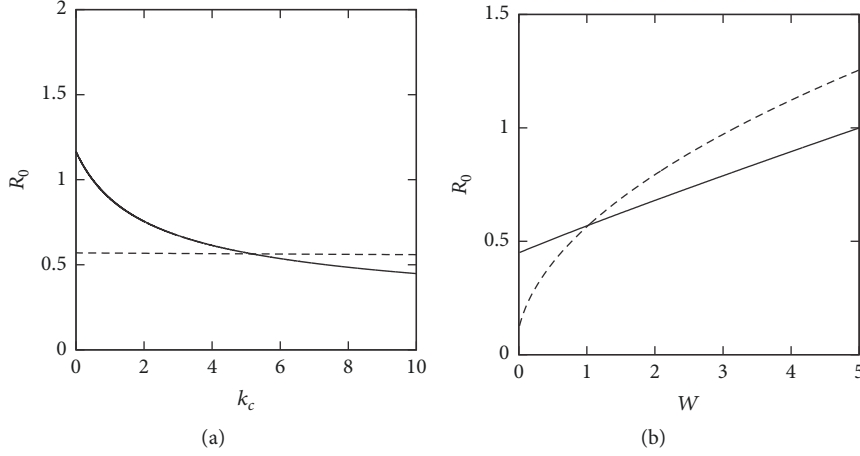
(34)

(35)

(a)

(b)

FIGURE 2: Dependence of R_0 on k_c and W in the stationary state. (a) Dependence of R_0 on k_c. $W = 1.0$. The solid and dashed curves represent the cases of $\alpha = 0$ and 5, respectively. (b) Dependence of R_0 on W. $k_c = 5.0$. The solid and dashed curves represent the cases of $\alpha = 0.1$ and 5.0, respectively.

with

$$G_q = \frac{1}{q^2 + \beta}. \tag{36}$$

In the above expansions, we omitted the term proportional to $(\mathbf{q} \cdot \mathbf{v})(\partial H_{\mathbf{q}}/\partial t)$ in the expressions of h_2 and $\widetilde{h}_2$. In the derivation of h_3 and $\widetilde{h}_3$, the terms proportional to $(\partial^3 H_{\mathbf{q}}/\partial t^3)$, $(\mathbf{q}\cdot\mathbf{v})(\partial^2 H_{\mathbf{q}}/\partial t^2)$, $(\mathbf{q}\cdot\mathbf{v})^2(\partial H_{\mathbf{q}}/\partial t)$, $(\mathbf{q}\cdot\dot{\mathbf{v}})(\partial H_{\mathbf{q}}/\partial t)$, $(\mathbf{q}\cdot\dot{\mathbf{v}})H_{\mathbf{q}}$, and $(\mathbf{q}\cdot\mathbf{v})(\mathbf{q}\cdot\dot{\mathbf{v}})H_{\mathbf{q}}$ were omitted. In the derivation of h_4 and $\widetilde{h}_4$, all the terms of the derivatives of $\mathbf{v}$ and $H_{\mathbf{q}}$ with respect to time were omitted. These terms were omitted, because they include higher order derivatives of time and are smaller than the remaining terms, or they vanish in the later integral $(1/\Omega) \int d\omega \mathbf{R}(\omega)\cdot$ due to the orthogonality relation of trigonometric functions. We remark that we include up to the third-order of $\mathbf{v}$: h_3 and $\widetilde{h}_3$, for the derivation of the equation of motion of the spot. The justification for considering terms up to this order is discussed later. On the other hand, for the derivation of equations of motion of tensors, we include up to the fourth order of $\mathbf{v}$: h_4 and $\widetilde{h}_4$. The justification for considering terms up to this order is discussed in Section 4.4.

When the spot is in a stationary motionless state, we assume that the spot is a circle with radius R_0. The values of v and $(\mathbf{n} \cdot \nabla)v$ at the interface are denoted as $h_0^{(0)}$ and $\widetilde{h}_0^{(0)}$, respectively. Using (34), $h_0^{(0)}$ is given by h_0 with the substitutions $H_{\mathbf{q}} = H_{\mathbf{q}}^{(0)}$ and $\mathbf{R} = \mathbf{R}^{(0)}$, where $\mathbf{R}^{(0)} = R_0\mathbf{e}_r$. Similarly, $\widetilde{h}_0^{(0)}$ is given using (35). When ϵ is small but finite, substituting $h = h_0^{(0)}$ and $\widetilde{h} = \widetilde{h}_0^{(0)}$ into $\tau C(h)$ with $V = 0$, (14) becomes

$$P\left(h_0^{(0)}\right) + Q\left(h_0^{(0)}\right)\widetilde{h}_0^{(0)} - \frac{\epsilon}{R_0} + L = 0, \tag{37}$$

where $\kappa = -1/R_0$ is used. We note that the Lagrange multiplier L in (37) can be absorbed into the constant term p_0 in $P(h_0^{(0)})$. In the limit $\epsilon \to 0$, we can calculate $h_0^{(0)}$ and

$\widetilde{h}_0^{(0)}$ by using $\overline{v}(r)$, which is given by (13) (the validation is given in Appendix B). Using these expressions, (37) gives the dependence of R_0 on k_c and W. The numerical results obtained by using (13) and (17) are shown in Figure 2(a). When $\alpha = 0$, R_0 monotonically decreases with k_c. However, for large α, R_0 depends weakly on k_c and it is almost constant because of the global coupling; large global coupling suppresses variations in the area of the spot resulting in constant R_0. The dependence of R_0 on W when k_c is large is shown in Figure 2(b). From (9), it can be seen that, for large α, R_0 approximately satisfies $\pi R_0^2 \sim W$, and, therefore, R_0 is proportional to the square root of W (see the dashed curve in Figure 2(b)).

When the spot moves with an infinitesimal velocity, h and $\widetilde{h}$ deviate from $h_0^{(0)}$ and $\widetilde{h}_0^{(0)}$, respectively. By putting small deviations as $\delta h = h - h_0^{(0)}$ and $\delta\widetilde{h} = \widetilde{h} - \widetilde{h}_0^{(0)}$, we iteratively derive δh and $\delta\widetilde{h}$ in a power series of τC up to the third order. The procedure consists of two steps. We first expand τC given by (17) in a power series of δh and $\delta\widetilde{h}$. Then, we solve the equation in terms of δh and expand it by τC. When the stationary motionless spot is destabilized into a moving spot, τC is expanded up to the second-order of δh and $\delta\widetilde{h}$ as

$$\tau C$$
$$= \left(\frac{\partial P}{\partial h} + \frac{\partial Q}{\partial h}\widetilde{h}_0^{(0)}\right)_0 \delta h + (Q)_0\, \delta\widetilde{h}$$
$$+ \frac{1}{2}\left[\left(\frac{\partial^2 P}{\partial h^2} + \frac{\partial^2 Q}{\partial h^2}\widetilde{h}_0^{(0)}\right)_0 \delta h^2 + 2\left(\frac{\partial Q}{\partial h}\right)_0 \delta h\delta\widetilde{h}\right], \tag{38}$$

where, for a function $A(h)$, $(A)_0$ implies $A(h_0^{(0)})$. Up to the first order of δh and $\delta\widetilde{h}$, (38) results in $\tau C = (\partial P/\partial h + \partial Q/\partial h\widetilde{h}_0^{(0)})_0\delta h + (Q)_0\delta\widetilde{h}$. For higher order corrections, a supplementary relation between δh and $\delta\widetilde{h}$ is necessary. In order to relate δh with $\delta\widetilde{h}$, we consider the profile of $v(\mathbf{r})$ in the radially symmetric function given by (13), where $v(\mathbf{r})$ is

a function of r $(= |\mathbf{r}|)$ denoted by $\bar{v}(r)$. For this function, $(\mathbf{n} \cdot \nabla)\bar{v} = d\bar{v}/dr$. Then, $\bar{v}(R_0 + \delta r)$ and $(\mathbf{n} \cdot \nabla)\bar{v}(R_0 + \delta r)$ are expanded around $\bar{v}(R_0)$ and $d\bar{v}(R_0)/dr$ for small δr as

$$\bar{v}(R_0 + \delta r) \sim \bar{v}(R_0) + \left(\frac{d\bar{v}}{dr}\right)_{r=R_0} \delta r, \tag{39}$$

$$(\mathbf{n} \cdot \nabla)\bar{v}(R_0 + \delta r) \sim \frac{d\bar{v}(R_0)}{dr} + \left(\frac{d^2\bar{v}}{dr^2}\right)_{r=R_0} \delta r, \tag{40}$$

respectively. In (39) and (40), $(A(r))_{r=R_0}$ implies $A(R_0)$. We make an ansatz that δh and $\delta\tilde{h}$ are not independent but have a linear relation such that $\delta\tilde{h} = k\delta h$ with $k = (\bar{v}''/\bar{v}')_{r=R_0}$, where the prime corresponds to the derivative with respect to r. This assumption enables us to calculate δh as a function of τC. Substituting $\delta\tilde{h} = k\delta h$ into (38), τC becomes a quadratic equation of δh as

$$\tau C = (a + kb)\,\delta h + m_1\delta h^2, \tag{41}$$

where

$$a = \left(\frac{\partial P}{\partial h} + \frac{\partial Q}{\partial h}\tilde{h}_0^{(0)}\right)_0,$$

$$b = (Q)_0, \tag{42}$$

$$m_1 = \frac{1}{2}\left[\left(\frac{\partial^2 P}{\partial h^2} + \frac{\partial^2 Q}{\partial h^2}\tilde{h}_0^{(0)}\right)_0 + 2k\left(\frac{\partial Q}{\partial h}\right)_0\right].$$

As a result of numerical calculations, we remark that $b > 0$ and $a < 0$ for small $h_0^{(0)}$, but $a > 0$ for large $h_0^{(0)}$. By solving (41) in terms of δh for small τC, the solution is expanded up to the second order of τC as

$$\delta h = \left(\frac{\tau C}{a + kb}\right) - \frac{m_1}{a + kb}\left(\frac{\tau C}{a + kb}\right)^2. \tag{43}$$

Here, it should be noted that although there are two solutions for (41), we chose one solution such that $\delta h \to \tau C/(a + kb)$ when the second-order term $(\tau C)^2$ is neglected.

In order to obtain δh up to the third order of τC, τC given by (17) is expanded up to the third order of δh and $\delta\tilde{h}$. Using $\delta\tilde{h} = k\delta h$, τC becomes a cubic equation of δh as

$$\tau C = (a + kb)\,\delta h + m_1\delta h^2 + m_2\delta h^3, \tag{44}$$

where m_2 is given by

$$m_2 = \frac{1}{6}\left[\left(\frac{\partial^3 P}{\partial h^3} + \frac{\partial^3 Q}{\partial h^3}\tilde{h}_0^{(0)}\right)_0 + 3k\left(\frac{\partial^2 Q}{\partial h^2}\right)_0\right]. \tag{45}$$

In order to obtain the third-order term of τC in δh, we add a correction Δ $(\sim O(\tau C)^3)$ to δh given by (43) and substitute it into (44). On solving this equation in terms of Δ, δh up to the third order of τC is obtained as

$$\delta h = \left(\frac{\tau C}{a + kb}\right) - \frac{m_1}{a + kb}\left(\frac{\tau C}{a + kb}\right)^2$$
$$+ \frac{1}{a + kb}\left[\frac{2m_1^2}{a + kb} - m_2\right]\left(\frac{\tau C}{a + kb}\right)^3. \tag{46}$$

We remark that (46) is obtained by another method; by applying Cardano's formula to (44) and expanding the solution up to the third order of τC, we obtain the same result as that of (46).

In the above process, we iteratively derived δh up to the third order of τC. We replace $k\delta h \sim \delta\tilde{h}$ in (46), and finally the power series expansion of $a\delta h + b\delta\tilde{h}$ in terms of τC is obtained as

$$a\delta h + b\delta\tilde{h} = M_1(\tau C) + M_2(\tau C)^2 + M_3(\tau C)^3, \tag{47}$$

where M_i $(i = 1, 2, 3)$ is defined by

$$M_1 = 1,$$

$$M_2 = -\frac{m_1}{(a + bk)^2}, \tag{48}$$

$$M_3 = \frac{1}{(a + bk)^3}\left[\frac{2m_1^2}{a + bk} - m_2\right].$$

In the absence of chemotaxis ($Q = 0$), (47) reproduces the result that was obtained in [16].

Using (14) and (47), we derive the equation of motion of the spot by operating both sides of (47) with $(1/\Omega)\int d\omega \mathbf{R}(\omega)$. For the left hand side, we put

$$\frac{1}{\Omega}\int d\omega \mathbf{R}(\omega)\,\delta h = \delta\mathbf{h} = \mathbf{h}_1 + \mathbf{h}_2 + \mathbf{h}_3,$$
$$\frac{1}{\Omega}\int d\omega \mathbf{R}(\omega)\,\delta\tilde{h} = \delta\tilde{\mathbf{h}} = \tilde{\mathbf{h}}_1 + \tilde{\mathbf{h}}_2 + \tilde{\mathbf{h}}_3, \tag{49}$$

where $\mathbf{h}_4$ and $\tilde{\mathbf{h}}_4$ are neglected because these terms are higher than or equal to $O(\mathbf{v}^4)$. For the calculation of the right hand side of (47), we use (14). The magnitudes of $\epsilon\kappa$ and L were discussed in [16]; L is independent of ϕ_r, and, owing to the periodicity of the function, $\int d\omega \mathbf{R}(\omega)L = \int d\omega \mathbf{R}(\omega)L^3 = \int d\omega \mathbf{R}(\omega)V^2L = 0$. In addition, $L \sim O(\mathbf{v}^2)$, and, therefore, $\int d\omega \mathbf{R}(\omega)VL^3$ can be neglected up to the third order of $\mathbf{v}$. As the translational motion of the spot is incorporated in $\boldsymbol{\rho}$, we chose $c_{\pm 1} = 0$ in the expansion of $\delta R(\phi_r)$. This results in $\epsilon\int d\omega \mathbf{R}(\omega)\kappa = 0$ up to the first order of the deformation. The terms $\epsilon\int d\omega \mathbf{R}(\omega)\kappa VL^2$ and $\epsilon\int d\omega \mathbf{R}(\omega)\kappa L^2$, and the higher order terms of ϵ were small; therefore, they were neglected. Following the above discussion, we neglect the term $(\epsilon\kappa + L)$ in (14).

By carrying the integral over ϕ_r, the following equation is obtained:

$$a\delta\mathbf{h} + b\delta\tilde{\mathbf{h}} = \tau\mathbf{v} + \frac{3}{4}M_3\tau^3\mathbf{v}|\mathbf{v}|^2, \tag{50}$$

where

$$\delta\mathbf{h} = \mathbf{h}_{1,1} + \mathbf{h}_{2,1} + \mathbf{h}_3,$$
$$\delta\tilde{\mathbf{h}} = \tilde{\mathbf{h}}_{1,1} + \tilde{\mathbf{h}}_{2,1} + \tilde{\mathbf{h}}_3. \tag{51}$$

Here, $\mathbf{h}_{1,1} = (1/\Omega)\int d\omega \mathbf{R}(\omega)h_{1,1}$. The other terms on the right hand side of (51) are defined similarly. In the expansion
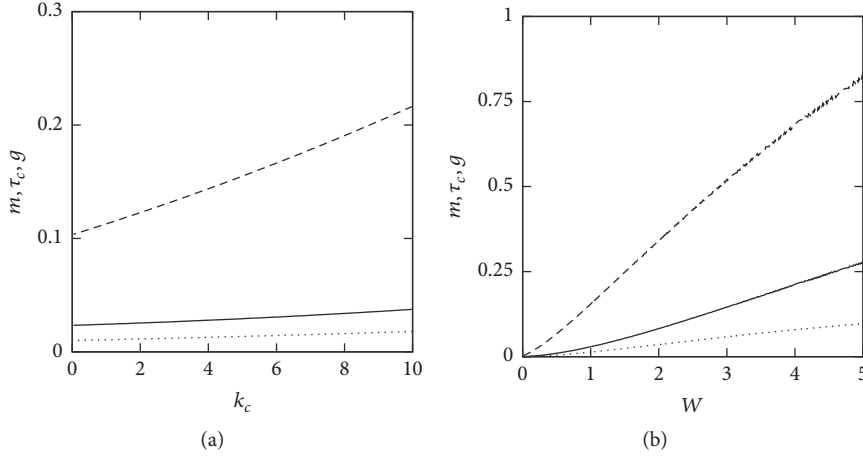
FIGURE 3: Dependence of m, τ_c, and g on k_c and W. The solid, dashed, and dotted curves represent m, τ_c, and g, respectively. (a) Dependence of m, τ_c, and g on k_c. $\alpha = 5.0$ and $W = 1.0$. In the calculation of g, τ is chosen as $\tau = \tau_c$. As M_3 is positive, g for the case $\tau < (>) \tau_c$ is smaller (larger) than this curve. (b) Dependence of m, τ_c, and g on W. $\alpha = 5.0$ and $k_c = 5.0$. In the calculation of g, τ is chosen as $\tau = \tau_c$.

(51), we neglected the terms $\mathbf{h}_{1,2}$ and $\mathbf{h}_{2,3}$, because these terms yielded only the terms $\dot{c}_{\pm 1}$ and $\ddot{c}_{\pm 1}$, respectively; however, these terms are set to zero. $\mathbf{h}_{2,2}$ disappeared in the integral over ϕ_r owing to the orthogonality relation of trigonometric functions [15]. Owing to the same reasons, the terms $\widetilde{\mathbf{h}}_{1,2}$, $\widetilde{\mathbf{h}}_{2,3}$, and $\widetilde{\mathbf{h}}_{2,2}$ did not exist. In the integral over ϕ_r, there is no contribution from the second-order term of τC owing to the orthogonality relation of trigonometric function. This supports the justification to include terms up to the third order of τC in (47) for the minimal equation of motion of a spot. For the balance of order, it is sufficient to include terms up to the third order of $\mathbf{v}$ in $\delta \mathbf{h}$ and $\delta \widetilde{\mathbf{h}}$.

After practical calculations of $\delta \mathbf{h}$ and $\delta \widetilde{\mathbf{h}}$, we finally obtain the equation of motion of the spot as

$$m\dot{\mathbf{v}} + (\tau - \tau_c)\,\mathbf{v} + g\mathbf{v}\,|\mathbf{v}|^2 = a\delta \mathbf{h}_{1,1}^{(0)} + b\delta \widetilde{\mathbf{h}}_{1,1}^{(0)}, \qquad (52)$$

where $\delta \mathbf{h}_{1,1}^{(0)}$ is defined as $\delta \mathbf{h}_{1,1}^{(0)} = \mathbf{h}_{1,1} - \mathbf{h}_{1,1}^{(0)}$. Here, $\mathbf{h}_{1,1}^{(0)}$ is given by $\mathbf{h}_{1,1}$ with the substitutions $H_{\mathbf{q}} = H_{\mathbf{q}}^{(0)}$ and $\mathbf{R} = \mathbf{R}^{(0)}$. $\delta \widetilde{\mathbf{h}}_{1,1}^{(0)}$ is similarly defined with $\delta \mathbf{h}_{1,1}^{(0)}$. The coefficients m, τ_c, and g on the left hand side of (52) are given by

$$m = -aR_0 F(1, 3, 1, 1) - bR_0 F_d(2, 3, 1, 1), \qquad (53)$$

$$\tau_c = -aR_0 F(1, 2, 1, 1) - bR_0 F_d(2, 2, 1, 1), \qquad (54)$$

$$g = \frac{3}{4}M_3\tau^3 - \frac{3}{4}aR_0 F(3, 4, 1, 1)$$
$$\qquad\qquad\qquad\qquad (55)$$
$$\quad - \frac{3}{4}bR_0 F_d(4, 4, 1, 1),$$

respectively, where we defined $F(i, j, k, l)$ and $F_d(i, j, k, l)$ as

$$F(i, j, k, l) = \int_0^\infty dq q^i G_q^j J_k J_l, \qquad (56)$$

$$F_d(i, j, k, l) = \int_0^\infty dq q^i G_q^j J_k \frac{\partial}{\partial(qR_0)}J_l, \qquad (57)$$

respectively, where i, j, k, and l are integers and $J_n(qR_0)$ is written as J_n for brevity.

Equation (52) has the same form as the one in the absence of chemotaxis [16]. It is a Newtonian equation of the spot; the effective mass m, damping coefficient τ_c, intensity of the cubic nonlinear term g, and the right hand side of (52) form the coupling term between deformation and velocity in the following subsection. When $(\tau - \tau_c) > 0$, the motionless spot is stable; however, the motionless spot is destabilized into a moving spot for $(\tau - \tau_c) < 0$. When g is positive, the third-order nonlinear coupling term $g\mathbf{v}|\mathbf{v}|^2$ suppresses the divergence for large $|\mathbf{v}|$. It is necessary that m, τ_c, and g are positive for the existence of a stable moving spot. The dependence of m, τ_c, and g on k_c and W is shown in Figure 3. We see that these parameters are positive and monotonically increase with k_c and W.

In the derivation of (47), we made an ansatz for the relation between δh and $\delta \widetilde{h}$ such that $\delta \widetilde{h} = k\delta h$ with $k = (\overline{v}''/\overline{v}')_{r=R_0}$. Equation (55) suggests that g depends explicitly on k through M_3. Through preliminary research, it is found that if k is chosen as a positive constant, the property that g is a positive and monotonically increasing function of k_c and W holds. From the above, it is seen that m, τ_c, and g are positive for any value of k_c and W, and, therefore, we fix W and examine the motion of the spot in the range $k_c \geq 0$.

4.3. Definitions of Tensors. In order to express the deformation of the spot, we introduce tensors. We rewrite the vector form (52) of each component, and, by denoting $\mathbf{v} = (v_1, v_2)$, the α component ($\alpha = 1, 2$) of (52) becomes

$$m\dot{v}_\alpha + (\tau - \tau_c)\,v_\alpha + gv_\alpha\,|\mathbf{v}|^2 = a\delta h_{1,1(\alpha)}^{(0)} + b\delta \widetilde{h}_{1,1(\alpha)}^{(0)}, \qquad (58)$$

where $\delta h_{1,1(\alpha)}^{(0)}$ and $\delta \widetilde{h}_{1,1(\alpha)}^{(0)}$ correspond to the α component of $\delta \mathbf{h}_{1,1}^{(0)}$ and $\delta \widetilde{\mathbf{h}}_{1,1}^{(0)}$, respectively. Using the tensors, the right hand side of (58) is expressed in a simple form. The second rank tensor $\mathbf{S}$ and the third rank tensor $\mathbf{U}$ represent the elliptical deformation and the head-tail asymmetric deformation

($2\pi/3$-periodic deformation in the radial direction) of the spot, respectively. These tensors are traceless and symmetric. The detailed definitions are given in [16]. The deformation $\delta R(\phi_r)$ is expanded using the coefficients c_n as given by (25); $c_{\pm n}$ corresponds to a $(2\pi/n)$-periodic deformation.

We first introduce a second-rank tensor $S_{\alpha\beta}$ ($\alpha, \beta = 1, 2$) using $c_{\pm 2}$ as follows:

$$S_{11} = -S_{22} = c_2 + c_{-2} = \frac{\delta_2}{2} \cos 2\phi_2,$$

$$S_{12} = S_{21} = i\left(c_2 - c_{-2}\right) = \frac{\delta_2}{2} \sin 2\phi_2,$$

(59)

where δ_2 is a positive constant, which represents the radial deviation of the spot from R_0, and ϕ_2 is the angle between the long axis of the ellipse and the x-axis. The tensor elements (59) are represented by using a normal vector $\mathbf{N} = (\cos\phi_2, \sin\phi_2)$ along the long axis as

$$S_{\alpha\beta} = \delta_2 \left(N_\alpha N_\beta - \frac{\delta_{\alpha\beta}}{2} \mathbf{N}^2 \right).$$

(60)

The tensor $\mathbf{S}$ is the same as the nematic order parameter tensor in liquid crystals [34]. For an elliptical spot, $R(\phi_r)$ is represented as

$$R(\phi_r) = R_0 + \frac{\delta_2}{2} \cos 2\left(\phi_r - \phi_2\right).$$

(61)

Next, in order to describe the head-tail asymmetric deformation, we first define T_1 and T_2 using $c_{\pm 3}$ as

$$T_1 = c_3 + c_{-3} = \delta_3 \cos 3\phi_3,$$

(62)

$$T_2 = i\left(c_3 - c_{-3}\right) = \delta_3 \sin 3\phi_3,$$

(63)

respectively, where δ_3 is a positive constant and ϕ_3 is the angle between one of the long axes of the deformed spot and the x-axis. In order to relate T_1 and T_2 with a tensor, we introduce the third-rank tensor $U_{\alpha\beta\gamma}$ ($\alpha, \beta,$ and $\gamma = 1$ or 2). The tensor elements $U_{\alpha\beta\gamma}$ are represented by using vectors $\mathbf{N}^{(m)}$ ($m = 1, 2,$ and 3) as

$$U_{\alpha\beta\gamma} = \frac{4\delta_3}{3} \sum_m N_\alpha^{(m)} N_\beta^{(m)} N_\gamma^{(m)},$$

(64)

where the normal vectors $\mathbf{N}^{(m)}$ are defined by

$$\mathbf{N}^{(1)} = \left(\cos\phi_3, \sin\phi_3\right),$$

$$\mathbf{N}^{(2)} = \left(\cos\left(\phi_3 + \frac{2\pi}{3}\right), \sin\left(\phi_3 + \frac{2\pi}{3}\right)\right),$$

$$\mathbf{N}^{(3)} = \left(\cos\left(\phi_3 - \frac{2\pi}{3}\right), \sin\left(\phi_3 - \frac{2\pi}{3}\right)\right).$$

(65)

The tensor $\mathbf{U}$ is the same as the order parameter for banana (tetrahedral nematic) liquid crystals in two dimensions [35, 36]. We obtain the relations between the tensor elements $U_{\alpha\beta\gamma}$ and T_1 and T_2 as $U_{111} = T_1$, $U_{222} = -T_2$, and

$$U_{111} = -U_{122} = -U_{212} = -U_{221},$$

$$U_{222} = -U_{112} = -U_{121} = -U_{211}.$$

(66)

The spot with head-tail asymmetric deformation is represented as

$$R(\phi_r) = R_0 + \delta_3 \cos 3\left(\phi_r - \phi_3\right).$$

(67)

The terms $\delta h_{1,1(\alpha)}^{(0)}$ and $\delta \widetilde{h}_{1,1(\alpha)}^{(0)}$ in (58) are expressed using tensors. The detailed calculations are given in Appendix C. The final form is as follows:

$$\delta h_{1,1(\alpha)}^{(0)} = -a^* \sum_\beta S_{\alpha\beta} v_\beta,$$

$$\delta \widetilde{h}_{1,1(\alpha)}^{(0)} = -\widetilde{a}^* \sum_\beta S_{\alpha\beta} v_\beta,$$

(68)

where

$$a^* = a_1^* + a_2^*,$$

$$a_1^* = -\frac{R_0}{2} F(2, 2, 1, 2),$$

(69)

$$a_2^* = -\frac{1}{2} \left[R_0 F(2, 2, 1, 2) - 3F(1, 2, 1, 1)\right],$$

(70)

$$\widetilde{a}^* = \widetilde{a}_1^* + \widetilde{a}_2^*,$$

$$\widetilde{a}_1^* = -\frac{R_0}{8} \left[-F(3, 2, 1, 2) + 3F(3, 2, 1, 1)\right]$$

$$- \frac{3}{4} F(2, 2, 0, 1),$$

(71)

$$\widetilde{a}_2^* = -2 \left[\frac{R_0}{4} F_d(2, 2, 2, 1) - F_d(1, 2, 1, 1)\right].$$

(72)

Thus, (58) is written using $S_{\alpha\beta}$ in the form

$$m\dot{v}_\alpha + (\tau - \tau_c) v_\alpha + g v_\alpha |\mathbf{v}|^2 = -\overline{a} \sum_\beta S_{\alpha\beta} v_\beta,$$

(73)

where $\overline{a} = (aa^* + b\widetilde{a}^*)$. $\delta h_{1,1(\alpha)}^{(0)}$ and $\delta \widetilde{h}_{1,1(\alpha)}^{(0)}$ yield the $\mathbf{Sv}$ term. This is due to the periodicity of the function in the integral over ϕ_r; in the expansion of $\delta \mathbf{R}(\phi_r)$ and $H_{\mathbf{q}}^{(1)}(\phi_r)$, only $c_{\pm 2}$ terms contribute to the nonzero integral, resulting in the $\mathbf{Sv}$ term. Equation (73) suggests that the motionless spot is destabilized into a moving spot for $\tau_c > \tau$, and the velocity of the spot is approximately given by $|\mathbf{v}|^2 \sim (\tau_c - \tau)/g$. The deformation and velocity coupling term $\mathbf{Sv}$ modifies the straight motion of the spot.

4.4. Time Evolution Equations of Tensors. In the previous subsection, we defined the tensors and described the equation of motion of the spot by using tensors, including the time-dependent tensor $S_{\alpha\beta}$. In this subsection, we derive the time evolution equations of the tensors up to $\sim O(\mathbf{v}^4)$. We first discuss the order of $\mathbf{v}$, $S_{\alpha\beta}$, and $U_{\alpha\beta\gamma}$, following [16]. From (73), the motionless spot is critical at $\tau = \tau_c$, and the moving spot occurs supercritically with increasing $(\tau_c - \tau)$. We put $\delta = \tau_c - \tau$ for the smallness parameter. The time is scaled by $\widehat{t} = t\delta$, an all the terms in (73) are of the order $O(\delta^{3/2})$.

Here $\mathbf{v} \sim O(\delta^{1/2})$ and $\mathbf{S} \sim O(\delta)$; therefore $S_{\alpha\beta} \sim O(\mathbf{v}^2)$. In the later calculations, we can confirm that $S_{\alpha\beta} \sim O(\mathbf{v}^2)$ and $U_{\alpha\beta\gamma} \sim O(\mathbf{v}^3)$. In the derivation of (73), we omitted the terms that include higher order derivatives of time. We estimate these terms, for example, $d^2\mathbf{v}/dt^2 \sim O(\delta^{5/2})$, $\mathbf{SSv} \sim O(\delta^{5/2})$, $(\mathbf{q} \cdot \mathbf{v})\partial H_\mathbf{q}/\partial t \sim O(\delta^{5/2})$, $\partial^3 H_\mathbf{q}/\partial t^3 \sim O(\delta^4)$, $(\mathbf{q} \cdot \mathbf{v})\partial^2 H_\mathbf{q}/\partial t^2 \sim O(\delta^{7/2})$, $(\mathbf{q} \cdot \mathbf{v})^2 \partial H_\mathbf{q}/\partial t \sim O(\delta^3)$, and $(\mathbf{q} \cdot \dot{\mathbf{v}})\partial H_\mathbf{q}/\partial t \sim O(\delta^{7/2})$ in the expansion of h and $\widetilde{h}$. From these estimates, the omission of those terms is justified.

$\mathbf{S}$ and $\mathbf{U}$ are composed of $c_{\pm 2}$ and $c_{\pm 3}$, respectively, so that $c_{\pm 2} \sim O(\mathbf{v}^2)$ and $c_{\pm 3} \sim O(\mathbf{v}^3)$. The coupling terms such as $c_n c_m$ ($|n|, |m| \geq 2$) are much smaller. Therefore, we linearize (14) in terms of the deformation δR. Then, the time evolution equation of δR becomes

$$\tau \frac{\partial \delta R}{\partial t} = \frac{\epsilon}{R_0^2} \left(\frac{\partial^2 \delta R}{\partial \phi_r^2} + \delta R \right) + a\delta h + b\delta\widetilde{h} + L. \tag{74}$$

We consider terms up to the fourth order of $\mathbf{v}$, where δh and $\delta\widetilde{h}$ are given by

$$\delta h = h - h_0^{(0)} = \delta h_0 + \delta h_1 + \delta h_2 + \delta h_3 + \delta h_4, \tag{75}$$

$$\delta\widetilde{h} = \widetilde{h} - \widetilde{h}_0^{(0)} = \delta\widetilde{h}_0 + \delta\widetilde{h}_1 + \delta\widetilde{h}_2 + \delta\widetilde{h}_3 + \delta\widetilde{h}_4, \tag{76}$$

respectively. Here, δh_0 and δh_l ($l = 1, 2, \ldots, 4$) are defined by (34) as $\delta h_0 = h_0 - h_0^{(0)}$ and $\delta h_l = h_l$, respectively. $\delta\widetilde{h}_l$ is similarly defined by (35). We expand δh_1, δh_2, $\delta\widetilde{h}_1$, and $\delta\widetilde{h}_2$ as $\delta h_1 = \delta h_{1,1} + \delta h_{1,2}$, $\delta h_2 = \delta h_{2,2}$, $\delta\widetilde{h}_1 = \delta\widetilde{h}_{1,1} + \delta\widetilde{h}_{1,2}$, and $\delta\widetilde{h}_2 = \delta\widetilde{h}_{2,2}$, respectively.

In order to derive the equation of motion of tensors, we calculate the first-order time derivative of c_n. The linear combination of $\dot{c}_n$ results in the equation of motion of tensors. In this process, $\dot{\mathbf{v}}$ terms in $\delta h_{2,1}$ and $\delta\widetilde{h}_{2,1}$ are neglected because these terms cause small order terms; $\sum_\gamma U_{\alpha\beta\gamma}\dot{v}_\gamma$ and $S_{\alpha\beta}\dot{v}_\gamma$ appear in the time evolution equation of $S_{\alpha\beta}$ and $U_{\alpha\beta\gamma}$, respectively. These terms are $\sum_\gamma U_{\alpha\beta\gamma}\dot{v}_\gamma \sim O(\mathbf{v}^6)$ and $S_{\alpha\beta}\dot{v}_\gamma \sim O(\mathbf{v}^5)$ so that they do not contribute to the equation of motion of tensors. In addition, $(\partial^2 H_\mathbf{q}/\partial t^2)$ terms in $\delta h_{2,3}$ and $\delta\widetilde{h}_{2,3}$ are neglected because these terms result in the second-order time derivative of c_n; these terms are $\ddot{c}_{\pm 2} \sim O(\mathbf{v}^6)$ and $\ddot{c}_{\pm 3} \sim O(\mathbf{v}^7)$ and they are small enough to be neglected.

We first derive the equation of motion of $S_{\alpha\beta}$. Using (74), we can obtain the time evolution equation of $c_{\pm 2}$, and we derive the time evolution equation of $S_{\alpha\beta}$. The detailed derivation is given in Appendices D and E. The time evolution equation of $S_{\alpha\beta}$ up to $O(\mathbf{v}^4)$ is

$$\Gamma_2 \frac{dS_{\alpha\beta}}{dt} = -K_2 S_{\alpha\beta} + \overline{b} \left[v_\alpha v_\beta - \frac{\delta_{\alpha\beta}}{2} |\mathbf{v}|^2 \right]$$
$$+ \overline{b}_s \left[v_\alpha v_\beta - \frac{\delta_{\alpha\beta}}{2} |\mathbf{v}|^2 \right] |\mathbf{v}|^2 + \overline{b}_1 \sum_\gamma U_{\alpha\beta\gamma} v_\gamma \tag{77}$$
$$+ \overline{c} |\mathbf{v}|^2 S_{\alpha\beta},$$

where $\Gamma_2 = \tau + aE_2 + b\widetilde{E}_2$, $K_2 = 3\epsilon/R_0^2 + aD_2 + b\widetilde{D}_2$, $\overline{b} = aG_1 + b\widetilde{G}_1$, $\overline{b}_s = -aG_1^s - b\widetilde{G}_1^s$, $\overline{b}_1 = -aB_3/2 + b(3\widetilde{A}^* - \widetilde{B}_3)/2$, and $\overline{c} = -a(2T_{2,2} - V_2) - b(2\widetilde{T}_{2,2} - \widetilde{V}_2)$. All the parameters in these expressions are given in Appendix E. The second term in (77) originates from δh_2 and $\delta\widetilde{h}_2$, the third term from δh_4 and $\delta\widetilde{h}_4$, the fourth term from δh_1 and $\delta\widetilde{h}_1$, and the fifth term from δh_2 and $\delta\widetilde{h}_2$. Thus, in order to consider the terms up to $O(\mathbf{v}^4)$, δh_4 and $\delta\widetilde{h}_4$ are necessary in the expansion equations (75) and (76). From the first and second terms in (77), we note that $S_{\alpha\beta} \sim O(\mathbf{v}^2)$.

Next, we consider the time evolution equation of $U_{\alpha\beta\gamma}$. Following procedures similar to those for $S_{\alpha\beta}$, the time evolution equation of $U_{\alpha\beta\gamma}$ up to $O(\mathbf{v}^4)$ is

$$\Gamma_3 \frac{dU_{\alpha\beta\gamma}}{dt} = -K_3 U_{\alpha\beta\gamma} + 4d_1 \left[v_\alpha v_\beta v_\gamma \right.$$
$$- \frac{|\mathbf{v}|^2}{4} \left(\delta_{\alpha\beta} v_\gamma + \delta_{\beta\gamma} v_\alpha + \delta_{\gamma\alpha} v_\beta \right) \right]$$
$$+ \frac{2d_2}{3} \left[S_{\alpha\beta} v_\gamma + S_{\beta\gamma} v_\alpha + S_{\gamma\alpha} v_\beta \right.$$
$$- \sum_\eta \frac{v_\eta}{2} \left(\delta_{\alpha\beta} S_{\gamma\eta} + \delta_{\beta\gamma} S_{\alpha\eta} + \delta_{\gamma\alpha} S_{\beta\eta} \right) \right], \tag{78}$$

where $\Gamma_3 = \tau + aE_3 + b\widetilde{E}_3$ and $K_3 = 8\epsilon/R_0^2 + aD_3 + b\widetilde{D}_3$. d_1 and d_2 are defined as

$$d_1 = -\frac{R_0}{4} \left[aF(3, 4, 1, 3) + bF_d(4, 4, 1, 3) \right], \tag{79}$$

$$d_2 = -a\frac{R_0}{2} \left[F(2, 2, 2, 3) + F_d(2, 2, 1, 1) \right]$$
$$- b\frac{R_0}{2} \left[F_d(3, 2, 2, 3) \right.$$
$$+ \frac{1}{4} \left(F(3, 2, 1, 3) - 3F(3, 2, 1, 1) \right) \right]$$
$$- \frac{b}{2} \left[F(2, 2, 0, 1) + F(2, 2, 1, 2) \right], \tag{80}$$

respectively. In the above equation, all the terms are $\sim O(\mathbf{v}^3)$. The terms of $O(\mathbf{v}^4)$ disappeared because of the orthogonality relation of trigonometric functions. The next higher order term is $O(\mathbf{v}^5)$, which is not included in expansions δh and $\delta\widetilde{h}$ in (75) and (76). The second term in (78) originates from δh_3 and $\delta\widetilde{h}_3$, and the third term from δh_1 and $\delta\widetilde{h}_1$. From the first and second terms in (78), we note that $U_{\alpha\beta\gamma} \sim O(\mathbf{v}^3)$.

5. Tensor Model

Using (73), (77), and (78), we discuss the stationary solution, the stability conditions of straight motion, and the critical

velocity of circular motion. For the sake of convenience, we rescale (73), (77), and (78) into

$$\frac{dv_\alpha}{dt} = \gamma v_\alpha - v_\alpha |\mathbf{v}|^2 - \bar{a}' \sum_\beta S_{\alpha\beta} v_\beta, \tag{81}$$

$$\frac{dS_{\alpha\beta}}{dt} = -\kappa S_{\alpha\beta} + \bar{b}' \left[v_\alpha v_\beta - \frac{1}{2} |\mathbf{v}|^2 \delta_{\alpha\beta} \right]$$

$$+ \bar{b}'_s \left[v_\alpha v_\beta - \frac{1}{2} |\mathbf{v}|^2 \delta_{\alpha\beta} \right] |\mathbf{v}|^2 \tag{82}$$

$$+ \bar{b}'_1 \sum_\gamma U_{\alpha\beta\gamma} v_\gamma + \bar{c}' |\mathbf{v}|^2 S_{\alpha\beta},$$

$$\frac{dU_{\alpha\beta\gamma}}{dt} = -K U_{\alpha\beta\gamma}$$

$$+ d'_1 \left[v_\alpha v_\beta v_\gamma - \frac{|\mathbf{v}|^2}{4} \left(\delta_{\alpha\beta} v_\gamma + \delta_{\beta\gamma} v_\alpha + \delta_{\gamma\alpha} v_\beta \right) \right]$$

$$+ \frac{d'_2}{3} \left[S_{\alpha\beta} v_\gamma + S_{\beta\gamma} v_\alpha + S_{\gamma\alpha} v_\beta \right] \tag{83}$$

$$- \sum_\eta \frac{v_\eta}{2} \left(\delta_{\alpha\beta} S_{\gamma\eta} + \delta_{\beta\gamma} S_{\alpha\eta} + \delta_{\gamma\alpha} S_{\beta\eta} \right) \Bigg],$$

respectively. We name (81)–(83) as the full tensor model [37]. In the above full tensor model, we chose parameters such that $g/m = 1$ and put $\gamma = (\tau_c - \tau)/m$ and $\bar{a}' = \bar{a}/m$ in (81). The other rescaled parameters in (82) and (83) were $\kappa = K_2/\Gamma_2$, $\bar{b}' = \bar{b}/\Gamma_2$, $\bar{b}'_s = \bar{b}_s/\Gamma_2$, $\bar{b}'_1 = \bar{b}_1/\Gamma_2$, $\bar{c}' = \bar{c}/\Gamma_2$, $K = K_3/\Gamma_3$, $d'_1 = 2d_1/\Gamma_3$, and $d'_2 = d_2/\Gamma_3$.

We summarize the coefficients in (81)–(83) as follows. γ is a damping coefficient in the time evolution equation of v_α; although the motionless spot is stable for $\gamma < 0$, the motionless spot is destabilized for $\gamma > 0$ and there appears a moving spot. κ and K are damping coefficients in the time evolution equations of $S_{\alpha\beta}$ and $U_{\alpha\beta\gamma}$, respectively. In this study, we fix K as a positive constant and consider κ in the range $\kappa > 0$. $\bar{b}'$ and $\bar{b}'_s$ are coefficients of the quadratic and fourth order of $\mathbf{v}$, respectively, in the time evolution equation of $S_{\alpha\beta}$. The term $\bar{b}'_s$ can be absorbed into $\bar{b}'$ with the replacement $\bar{b}' \to (\bar{b}' + \bar{b}'_s |\mathbf{v}|^2)$. From the results, it can be seen that the term $\bar{b}'$ is enhanced (suppressed) when the sign of $\bar{b}'_s$ is the same as (different from) that of $\bar{b}'$. d'_1 is the coefficient of the cubic term of $\mathbf{v}$ in the time evolution equation of $U_{\alpha\beta\gamma}$. These terms cause deformations with increasing velocity. The other parameters are coupling coefficients of deformation and velocity. $\bar{a}'$ and d'_2 are the coupling coefficients of $S_{\alpha\beta} v_\beta$ and $S_{\alpha\beta} v_\gamma$, respectively, and these terms influence the time evolution of v_α and $U_{\alpha\beta\gamma}$, respectively. $\bar{b}'_1$ and $\bar{c}'$ are the coupling coefficients of $U_{\alpha\beta\gamma} v_\gamma$ and $|\mathbf{v}|^2 S_{\alpha\beta}$, respectively. When $\bar{b}'_1 = 0$, $U_{\alpha\beta\gamma}$ is decoupled from v_α and $S_{\alpha\beta}$. $\bar{c}' |\mathbf{v}|^2 S_{\alpha\beta}$ can be absorbed into $-\kappa S_{\alpha\beta}$ with the

replacement $\kappa \to (\kappa - \bar{c}' |\mathbf{v}|^2)$. Then, the term κ is suppressed (enhanced) when $\bar{c}'$ is positive (negative), with $|\mathbf{v}|^2 \neq 0$.

The dependence of $\bar{a}'$, $\bar{b}'$, $\bar{b}'_s$, $\bar{c}'$, $\bar{b}'_1$, d'_1, and d'_2 on k_c is shown in Figure 4. In each figure, these parameters (shown on the vertical axis) are scaled by R_0^2. We see that both $\bar{a}'$ and $\bar{b}'$ are negative, and $\bar{b}'_1, \bar{c}' \neq 0$ even at $k_c = 0$. Although $\bar{b}'_1$ is a monotonically increasing function of k_c, $\bar{c}'$ is a monotonically decreasing function of k_c. d'_1 and d'_2 are positive but d'_1 is much smaller than d'_2.

Henceforth, we drop the primes on the parameters in the full tensor model (81)–(83). In the full tensor model, when K is large and $\mathbf{v}$ is small, the effect of $U_{\alpha\beta\gamma}$ on $S_{\alpha\beta}$ is small in (82). In this case, we put $\bar{b}_1 = 0$, and the v_α, $S_{\alpha\beta}$, and $U_{\alpha\beta\gamma}$ system described by (81)–(83) is reduced to a v_α and $S_{\alpha\beta}$ system. We call this system the reduced tensor model.

6. Stationary Solution and Phase Diagrams

In the following subsections, we consider the stationary solution and phase diagrams. For this, we rewrite v_α, $S_{\alpha\beta}$, and $U_{\alpha\beta\gamma}$ by introducing the following variables:

$$v_1 = v \cos\phi,$$

$$v_2 = v \sin\phi,$$

$$S_{11} = \frac{s}{2} \cos 2\theta,$$

$$S_{12} = \frac{s}{2} \sin 2\theta, \tag{84}$$

$$U_{111} = c_3 + c_{-3},$$

$$U_{222} = -i \left(c_3 - c_{-3} \right),$$

$$c_{\pm 3} = \frac{\delta_3}{2} e^{\mp i 3\phi_3} \equiv \frac{z}{4} e^{\mp i 3\varphi},$$

where we choose $v, s, z > 0$. From (81), we obtain the time evolution equations of v and ϕ as

$$\frac{d}{dt} v = v \left(\gamma - v^2 \right) - \frac{1}{2} \bar{a} s v \cos 2 \left(\theta - \phi \right), \tag{85}$$

$$\frac{d}{dt} \phi = -\frac{1}{2} \bar{a} s \sin 2 \left(\theta - \phi \right), \tag{86}$$

respectively. From (82), we obtain the time evolution equations of s and θ as

$$\frac{d}{dt} s = -\kappa s + \bar{b} v^2 \cos 2 \left(\theta - \phi \right) + \bar{b}_s v^4 \cos 2 \left(\theta - \phi \right)$$

$$+ \bar{b}_1 z v \cos \left(2\theta + \phi - 3\varphi \right) + \bar{c} v^2 s, \tag{87}$$

$$\frac{d}{dt} \theta = -\frac{\bar{b} v^2}{2s} \sin 2 \left(\theta - \phi \right) - \frac{\bar{b}_s v^4}{2s} \sin 2 \left(\theta - \phi \right)$$

$$+ \frac{\bar{b}_1 z v}{2s} \sin \left(3\varphi - \phi - 2\theta \right), \tag{88}$$
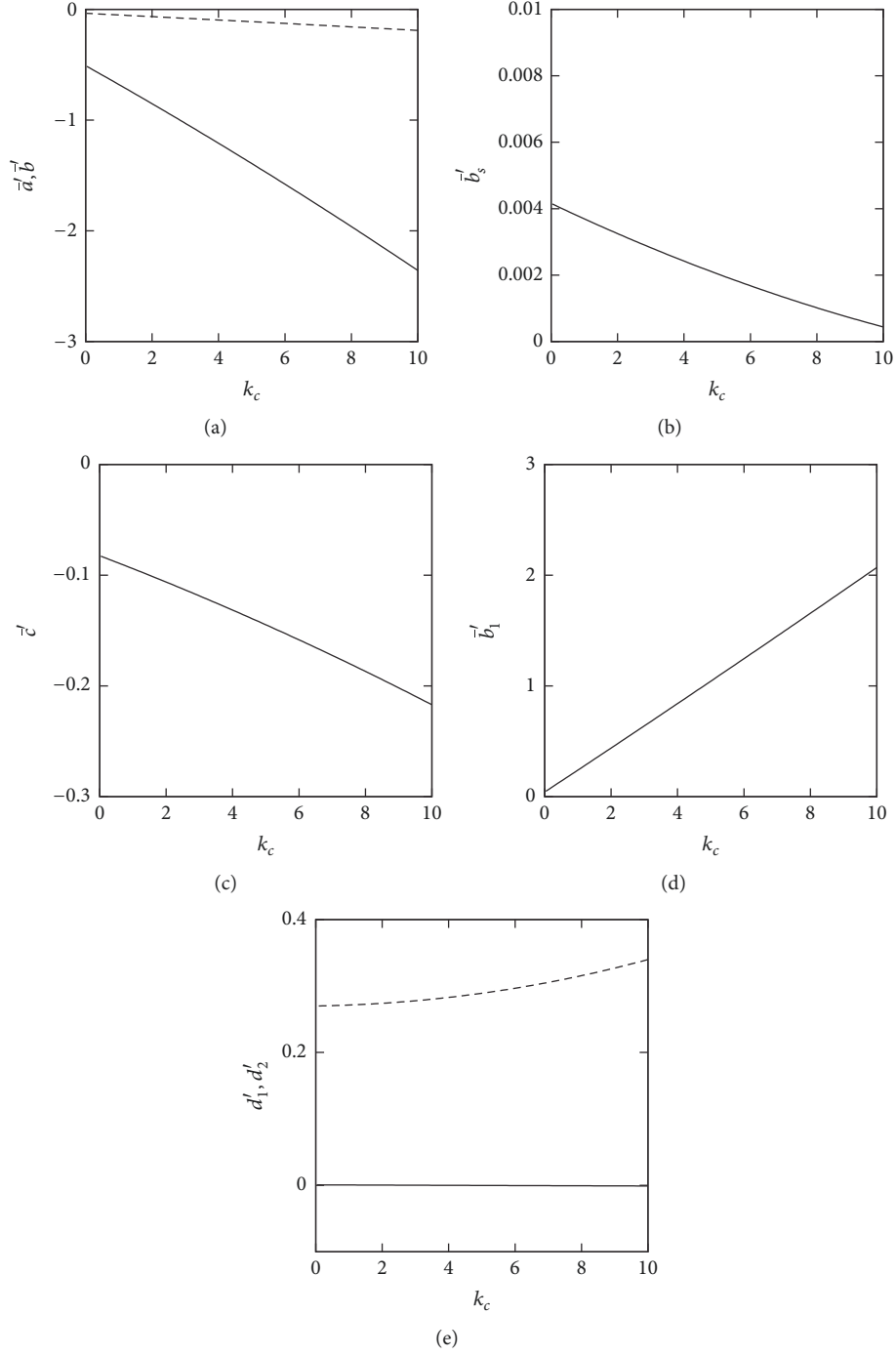
(a)

(b)

(c)

(d)

(e)

FIGURE 4: Dependence of $\bar{a}'$, $\bar{b}'$, $\bar{b}'_s$, $\bar{c}'$, $\bar{b}'_1$, d'_1, and d'_2 on k_c. $\alpha = 5.0$ and $W = 1.0$. All the parameters in the vertical axis are scaled by R_0^2. (a) $\bar{a}'$ and $\bar{b}'$. The solid and dashed curves represent $\bar{a}'$ and $\bar{b}'$, respectively. (b) $\bar{b}'_s$. (c) $\bar{c}'$. (d) $\bar{b}'_1$. (e) d'_1 and d'_2. The solid and dashed curves represent d'_1 and d'_2, respectively.

respectively. From (83), we obtain the time evolution equations of z and φ as

$$\frac{d}{dt}z = -Kz + d_1 v^3 \cos 3\left(\varphi - \phi\right) + d_2 sv \cos\left(3\varphi - 2\theta - \phi\right), \tag{89}$$

$$\frac{d}{dt}\varphi = -\frac{d_1}{3z}v^3 \sin 3\left(\varphi - \phi\right) - \frac{d_2}{3z}sv \sin\left(3\varphi - 2\theta - \phi\right). \tag{90}$$

Using (85)–(90), we theoretically derive the stationary solution and phase diagrams. In order to verify the theoretical

result, we perform simulations of the reduced tensor model. For the numerical calculations, we employ the fourth-order Runge-Kutta algorithm with the time increment $\Delta t = 1.0 \times 10^{-4}$ and fix the parameters as $\bar{a} = \bar{b} = -1$, $K = 0.3$, $d_1 = 0.1$, and $d_2 = 0.5$.

6.1. Stationary Solution.

For the reduced and full tensor models, we consider the stationary solution of the moving spot, which moves straight in the x direction. This situation corresponds to $\phi = 0$. In the case of $\bar{b}_1 = \bar{b}_s = \bar{c} = 0$, the stationary solution of (85) and (86) becomes $v_0^2 = \gamma/(1 + B)$ with $B = \bar{a}\bar{b}/2\kappa$. In order to avoid the divergence of v_0^2, we assume that $\bar{a}\bar{b} > 0$. For $\bar{c} \neq 0$, we consider the dependence of the stationary solution of s, z, θ, and φ on the signs of $\bar{a}$ and $\bar{b}$. In the stationary state of (86) with $\phi = 0$, there are two stationary solutions of θ depending on the sign of $\bar{a}$ and $\bar{b}$: (I) $\bar{a}$ and $\bar{b}$ are positive with $\theta_0 = l\pi$ and (II) $\bar{a}$ and $\bar{b}$ are negative with $\theta_0 = (l + 1/2)\pi$, where l is an integer. Using (87)–(90), the stationary solution of case (I) is

$$s_0 = \left[\frac{\left(\bar{b} + \bar{b}_s v_0^2\right) K + \bar{b}_1 d_1 v_0^2}{K\left(\kappa - \bar{c}v_0^2\right) - d_2 \bar{b}_1 v_0^2} \right] v_0^2,$$

$$z_0 = \cos 3\varphi_0 \left[\frac{d_1\left(\kappa - \bar{c}v_0^2\right) + d_2\left(\bar{b} + \bar{b}_s v_0^2\right)}{K\left(\kappa - \bar{c}v_0^2\right) - d_2 \bar{b}_1 v_0^2} \right] v_0^3, \qquad (91)$$

where φ_0 satisfies $\sin 3\varphi_0 = 0$ and v_0 is a stationary solution of v, which is determined later. On the other hand, for case (II), the stationary solution is

$$s_0 = -\left[\frac{\left(\bar{b} + \bar{b}_s v_0^2\right) K + \bar{b}_1 d_1 v_0^2}{K\left(\kappa - \bar{c}v_0^2\right) - d_2 \bar{b}_1 v_0^2} \right] v_0^2,$$

$$z_0 = \cos 3\varphi_0 \left[\frac{d_1\left(\kappa - \bar{c}v_0^2\right) + d_2\left(\bar{b} + \bar{b}_s v_0^2\right)}{K\left(\kappa - \bar{c}v_0^2\right) - d_2 \bar{b}_1 v_0^2} \right] v_0^3. \qquad (92)$$

From these results, it is seen that z_0 has the same expression irrespective of the signs of $\bar{a}$ and $\bar{b}$. As z_0 is positive, φ_0 satisfying $\sin 3\varphi_0 = 0$ is chosen as

(i) $\varphi_0 = \dfrac{2m}{3}\pi$,

if $\left[\dfrac{d_1\left(\kappa - \bar{c}v_0^2\right) + d_2\left(\bar{b} + \bar{b}_s v_0^2\right)}{K\left(\kappa - \bar{c}v_0^2\right) - v_0^2 d_2 \bar{b}_1} \right] > 0$,

(ii) $\varphi_0 = \dfrac{(2m + 1)}{3}\pi$,   (93)

if $\left[\dfrac{d_1\left(\kappa - \bar{c}v_0^2\right) + d_2\left(\bar{b} + \bar{b}_s v_0^2\right)}{K\left(\kappa - \bar{c}v_0^2\right) - v_0^2 d_2 \bar{b}_1} \right] < 0$.

For both cases ((I) and (II)), the stationary solution of z_0 is given by

$$z_0 = \left| \frac{d_1\left(\kappa - \bar{c}v_0^2\right) + d_2\left(\bar{b} + \bar{b}_s v_0^2\right)}{K\left(\kappa - \bar{c}v_0^2\right) - d_2 \bar{b}_1 v_0^2} \right| v_0^3. \qquad (94)$$

In both cases ((I) and (II)), by substituting s_0 into (85) in the stationary state, we obtain two stationary solutions $v_{0,\pm}$ as

$$v_{0,\pm}^2 = \frac{1}{f_1}\left[f_2 \pm \sqrt{f_3} \right]$$

with $f_1 = 2\left[K\bar{c} + d_2 \bar{b}_1 - \frac{1}{2}\bar{a}\left(\bar{b}_1 d_1 + K\bar{b}_s\right) \right]$,

$$f_2 = \left(\frac{1}{2}\bar{a}\bar{b} + \kappa + \gamma\bar{c}\right)K + \gamma d_2 \bar{b}_1, \qquad (95)$$

$$f_3 = \left[\left(\frac{1}{2}\bar{a}\bar{b} - \kappa + \gamma\bar{c}\right)K + \gamma d_2 \bar{b}_1 \right]^2 + 2\bar{a}\kappa\left[\left(\bar{b} + \bar{b}_s\gamma\right)K^2 + \gamma\bar{b}_1 d_1 K \right].$$

In order to satisfy the condition that $v_{0,\pm}^2 \to \gamma/(1 + B)$ in the limits $\bar{b}_1, \bar{b}_s$, and $\bar{c} \to 0$, only $v_{0,-}^2$ exists. In the physical images of the moving spot in cases (I) and (II) with $\varphi_0 = 0$, the long axes of the elliptical domain are parallel and perpendicular to the moving direction, respectively [16].

6.2. Stability of Straight Motion in the Reduced Tensor Model.

When K is large in (89), z is rapidly damped to zero. In addition, when v is small, the influences of z on s and θ in (87) and (88) are small. For this case, we discuss the stability of the straight motion of the spot by setting $\bar{b}_1 = 0$ in (87) and (88). Using (86) and (88), we can derive the time evolution equation of $\psi = \theta - \phi$ as

$$\frac{d\psi}{dt} = -\frac{1}{2}\left(-\bar{a}s + \frac{\bar{b}v^2}{s} + \frac{\bar{b}_s v^4}{s} \right)\sin 2\psi. \qquad (96)$$

For the stationary states $v = v_{0,-}$, $s = s_0$, we discuss the stability condition of the straight motion. From (96), the stationary solution ψ_0 satisfies $2\psi_0 = 2l\pi$ or $(2l + 1)\pi$, and their corresponding stability conditions are $(-\bar{a}s_0 + \bar{b}v_{0,-}^2/s_0 + \bar{b}_s v_{0,-}^4/s_0) > 0$ or $(-\bar{a}s_0 + \bar{b}v_{0,-}^2/s_0 + \bar{b}_s v_{0,-}^4/s_0) < 0$, respectively. Since $\bar{a}$ and $\bar{b}$ are negative in our RD system, as shown in Figure 4(a), we consider the case of $\psi_0 = \pi/2$ as follows.
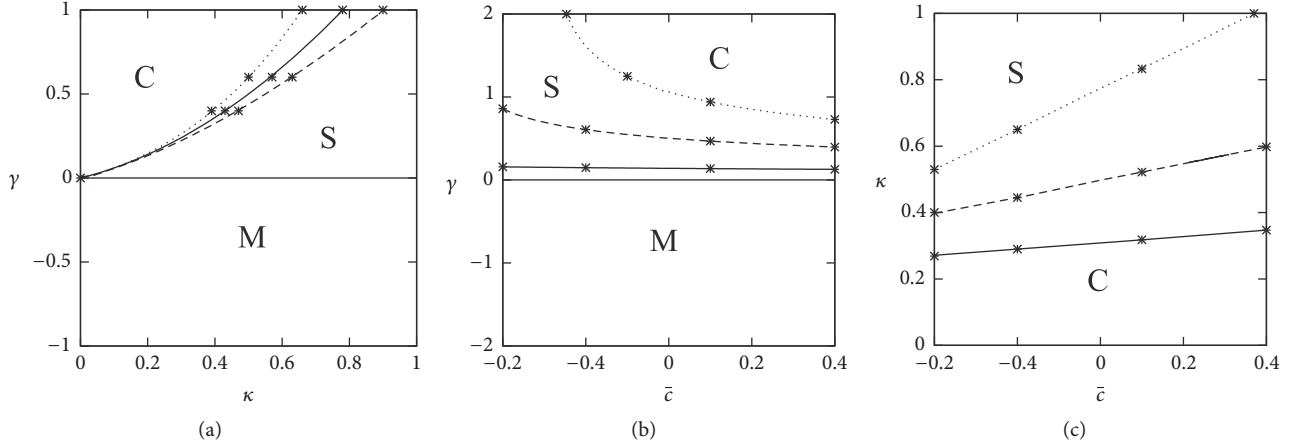
(a)　　　　　　　　　　　　(b)　　　　　　　　　　　　(c)

FIGURE 5: Phase diagram of spot motion. $\bar{a} = \bar{b} = -1$ and $\bar{b}_s = 0.05$. Data are obtained by the analysis of (96). M, S, and C in the figure represent regions of no motion, straight motion, and circular motion, respectively. The mark $*$ represents the data obtained by the simulation of the reduced tensor model. (a) Phase diagram in the κ-γ plane. The solid, dashed, and dotted curves correspond to the cases of $\bar{c} = 0$, 0.2, and −0.2, respectively. The upper (lower) region of each curve corresponds to the region of circular (straight) motion, and the region $\gamma \leq 0$ corresponds to the region of no motion. (b) Phase diagram in the $\bar{c}$-γ plane. The solid, dashed, and dotted curves correspond to cases of $\kappa = 0.2$, 0.5, and 0.8, respectively. The region across each curve is the same as in (a). (c) Phase diagram in the $\bar{c}$-κ plane. The solid, dashed, and dotted curves correspond to the cases of $\gamma = 0.25$, 0.5, and 1.0, respectively. The upper (lower) region of each curve corresponds to the region of straight (circular) motion.

In this case, the stability condition is calculated using the s_0 given by (92). The bifurcation of straight-circular motion, when $\bar{b}_s = \bar{c} = 0$, was already studied in [16], and the critical value for the straight motion is expressed as

$$\gamma_c = \frac{\kappa^2}{\bar{a}\bar{b}} + \frac{\kappa}{2}. \tag{97}$$

The phase diagram in the κ-γ plane is shown by the solid curve in Figure 5(a). When $\gamma \leq 0$, the motionless spot is stable. When γ is in the range $0 < \gamma \leq \gamma_c$, the spot moves straight. However, when $\gamma > \gamma_c$, the straight motion become unstable and changes into circular motion. On the other hand, when $\bar{b}_s \neq 0$ and $\bar{c} \neq 0$, the stability condition for straight motion is

$$\bar{a}\left[\frac{\bar{b}v_{0,-}^2 + \bar{b}_s v_{0,-}^4}{\kappa - \bar{c}v_{0,-}^2}\right] < \kappa - \bar{c}v_{0,-}^2. \tag{98}$$

The phase diagram is a curved surface in κ-γ-$\bar{c}$ space; the boundary of different motions of spot is obtained by using (98). The phase diagram in the κ-γ plane is shown in Figure 5(a) with dashed and dotted curves. Comparing the curves with that for the case when $\bar{b}_s = \bar{c} = 0$ (the solid curve), it can be seen that when $\bar{c} > 0$, the parameter region for the circular motion is larger. However, when $\bar{c} < 0$, the parameter region for the circular motion is smaller. We can explain this result using (87); the term $\bar{c}v^2 s$ essentially reduces the parameter κ of the damping term $-\kappa s$ such that the damping term becomes $-(\kappa - \bar{c}v^2)s$. When $\bar{c}$ is positive (negative), the term $\bar{c}v^2 s$ effectively reduces (increases) κ so that the deformation s becomes large (small). This leads to positive (negative) $\bar{c}$ results in the larger parameter region

of the circular motion. In our RD system, $\bar{c}$ is negative and $|\bar{c}|$ monotonically increases with k_c (see Figure 4(c)), and the parameter region for circular motion becomes smaller as the intensity of chemotaxis increases. The phase diagrams in the $\bar{c}$-γ plane and $\bar{c}$-κ plane are shown in Figures 5(b) and 5(c), respectively. Figure 5(b) suggests that the parameter region for the circular motion is smaller for a larger value of κ. Equation (87) suggests that a larger value of κ damps s strongly such that the deformation is small, resulting in a smaller region of the circular motion. On the other hand, Figure 5(c) suggests that the parameter region for the circular motion is larger for a larger value of γ. Equation (85) suggests that a large positive value of γ enhances v such that the deformation becomes large, resulting in a larger region of circular motion. In each figure, the simulation results for the reduced tensor model are shown; they agree well with the theoretical results.

6.3. Dependence of Critical Velocity on Parameters.
In the previous subsection, we showed that a spot appears in the circular motion when $\gamma > \gamma_c$. In this parameter region, we examine the stationary circular motion of the spot with a constant angular frequency ω and velocity v_r. For this, we set $\bar{b}_1 = 0$ and substitute $v = v_r$, $s = s_r$, $\theta = \omega t + \zeta/2$, and $\phi = \omega t$ into (85)–(88), and obtain the relations among ζ, s_r, v_r, and ω. The calculation is straightforward; the final expressions are shown.

We first consider the case when $\bar{b}_s = \bar{c} = 0$, where up to $O(\mathbf{v}^3)$ terms are considered, and obtain the relations $\cos\zeta = \kappa/\bar{a}s_r$, $s_r^2 = \bar{b}v_r^2/\bar{a}$, $v_r^2 = (\gamma-\kappa/2)$, $\omega^2 = (\bar{a}\bar{b}/4)(v_r^2-v_c^2)$, and $v_c^2 = \kappa^2/\bar{a}\bar{b}$. When the spot rotates with an angular frequency ω, ω satisfies $\omega^2 \geq 0$, and this condition leads to $v_r \geq v_c$ [16]. The dependence of the critical velocity v_c for the stable angular
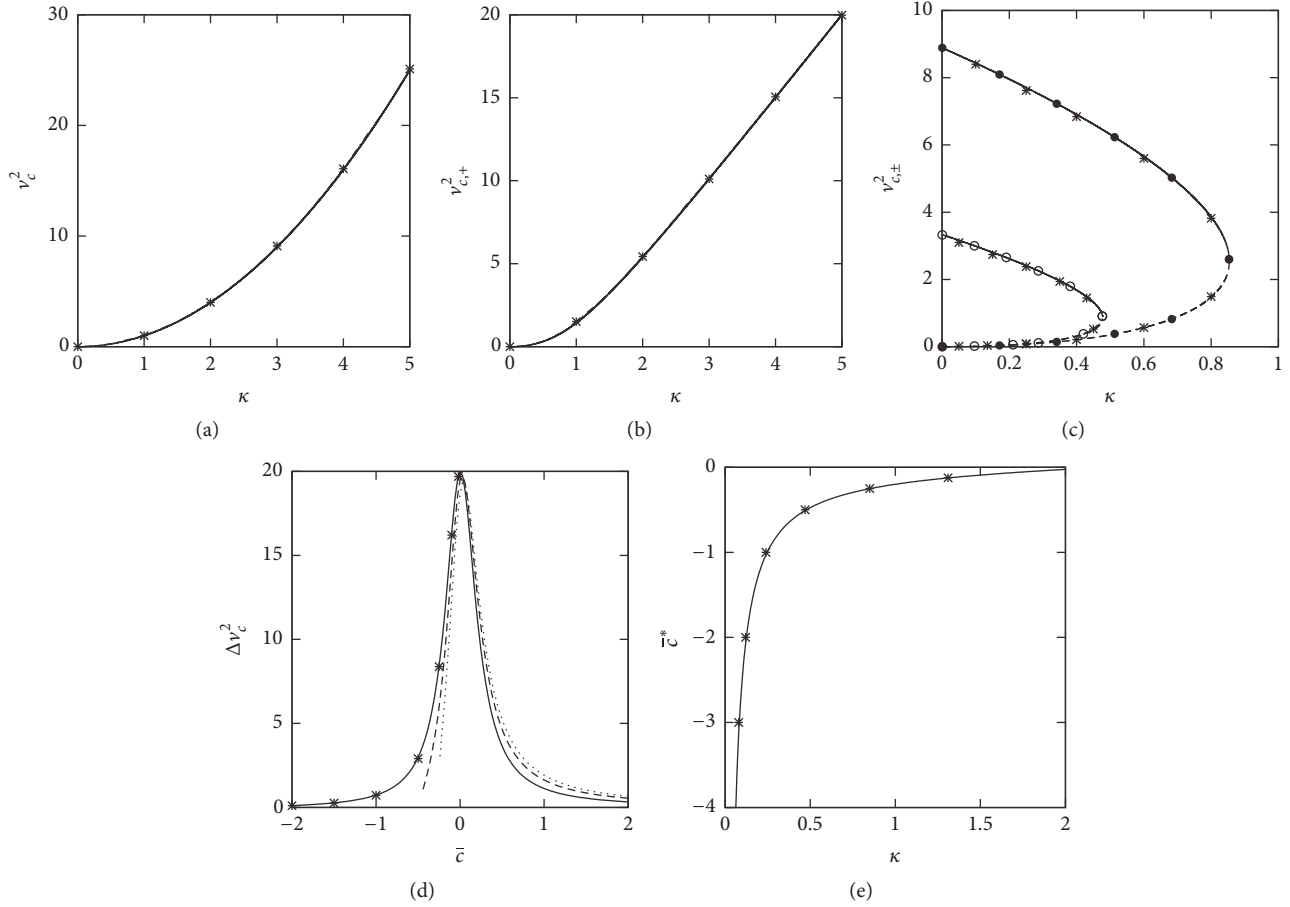
FIGURE 6: Dependence of the critical velocity v_c, $v_{c,\pm}$, Δv_c^2, and $\bar{c}^*$ on κ and $\bar{c}$. $\bar{a} = \bar{b} = -1$. The mark $*$ represents data obtained by the simulation of the reduced tensor model. (a) Dependence of v_c^2 on κ. $\bar{b}_s = \bar{c} = 0$. (b) Dependence of $v_{c,+}^2$ on κ. $\bar{b}_s = -0.2$ and $\bar{c} = -0.25$. (c) Dependence of $v_{c,\pm}^2$ on κ. $\bar{b}_s = 0.05$. The curves with filled (•) and open (○) circles correspond to the cases of $\bar{c} = -0.25$ and $\bar{c} = -0.5$, respectively. The solid and dashed curves represent $v_{c,-}^2$ and $v_{c,+}^2$, respectively. (d) Dependence of Δv_c^2 on $\bar{c}$. $\bar{b}_s = 0.05$. The solid, dashed, and dotted curves correspond to $\kappa = 0.1$, 0.5, and 0.8, respectively. (e) Dependence of $\bar{c}^*$ on κ. $\bar{b}_s = 0.05$.

frequency on κ (≥ 0) is shown in Figure 6(a). In this case, there is a lower limit of velocity v_c for the circular motion but no upper limit of velocity for the same.

Next, we consider the case when $\bar{b}_s \neq 0$ and $\bar{c} \neq 0$, where up to $O(\mathbf{v}^4)$ terms are considered. After similar calculations to the case of $\bar{b}_s = \bar{c} = 0$, we obtain the relations $\cos\zeta = (\kappa - \bar{c}v_r^2)/\bar{a}s_r$, $s_r^2 = (\bar{b}v_r^2 + \bar{b}_s v_r^4)/\bar{a}$, $v_r^2 = (\gamma - \kappa/2)/(1 - \bar{c}/2)$, and $\omega^2 = (\bar{a}\bar{b}_s - \bar{c}^2)v_r^4/4 + (\bar{a}\bar{b} + 2\kappa\bar{c})v_r^2/4 - \kappa^2/4$. In this case, ω^2 is a quartic function of v_r. For the condition $\omega^2 \geq 0$, there are two cases depending on the sign of $(\bar{a}\bar{b}_s - \bar{c}^2)$. When $(\bar{a}\bar{b}_s - \bar{c}^2) > 0$, ω^2 exists for $v_r^2 \geq v_{c,+}^2$, where $v_{c,\pm}^2$ are the solutions of $\omega^2 = 0$, which are given by $v_{c,\pm}^2 = [-(\bar{a}\bar{b} + 2\kappa\bar{c}) \pm \sqrt{D_r}]/[2(\bar{a}\bar{b}_s - \bar{c}^2)]$ with $D_r = (\bar{a}\bar{b} + 2\kappa\bar{c})^2 + 4\kappa^2(\bar{a}\bar{b}_s - \bar{c}^2)$. The dependence of $v_{c,+}^2$ on κ is shown in Figure 6(b); there is only a lower limit of velocity $v_{c,+}$. This property is the same with the case when $\bar{b}_c = \bar{c} = 0$. On the other hand, when $(\bar{a}\bar{b}_s - \bar{c}^2) < 0$, ω^2 exists in a certain range of v_r^2; $v_{c,+}^2 \leq v_r^2 \leq v_{c,-}^2$ under the condition $D_r \geq 0$. In this case, there is a lower limit and an upper limit of

velocity, $v_{c,+}$ and $v_{c,-}$, respectively. The gap between $v_{c,-}^2$ and $v_{c,+}^2$ is defined by $\Delta v_c^2 = v_{c,-}^2 - v_{c,+}^2 = \sqrt{D_r}/(\bar{c}^2 - \bar{a}\bar{b}_s)$. Let us consider two limiting cases. In the limit $|\bar{c}| \to \infty$, $v_{c,\pm}^2$ and $\Delta v_c^2 \to 0$. That is, the circular motion cannot exist. On the other hand, for small $|\bar{c}|$ and $|\bar{b}_s| \ll 1$, we expand $v_{c,\pm}^2$ in terms of $\bar{c}$ and $\bar{b}_s$ and obtain $v_{c,+}^2 \sim \kappa^2/(\bar{a}\bar{b} + 2\kappa\bar{c})$ and $v_{c,-}^2 \sim (\bar{a}\bar{b} + 2\kappa\bar{c})/(\bar{c}^2 - \bar{a}\bar{b}_s)$. Thus, in the limits $\bar{b}_s$ and $\bar{c} \to 0$, $v_{c,+}^2 \to \kappa^2/\bar{a}\bar{b}$, $v_{c,-}^2 \to \infty$, and $\Delta v_c^2 \to \infty$. This suggests that $v_{c,+} \to v_c$ and there is no upper limit of velocity, which are the same with the case when $\bar{b}_s = \bar{c} = 0$. From the numerical results shown in Figures 4(a), 4(b), and 4(c), $(\bar{a}\bar{b}_s - \bar{c}^2) < 0$ in our RD system; therefore, it turns out that v_r^2 exists only in a finite range, $v_{c,+}^2 \leq v_r^2 \leq v_{c,-}^2$. For larger $|\bar{c}|$, the gap $\Delta v_{c,\pm}^2$ is smaller, as shown in Figure 6(c). The dependence of Δv_c^2 on $\bar{c}$ is shown in Figure 6(d), which suggests that Δv_c^2 monotonically decreases with increasing $|\bar{c}|$. Since $|\bar{c}|$ increases monotonically as k_c increases (Figure 4(c)), Δv_c^2
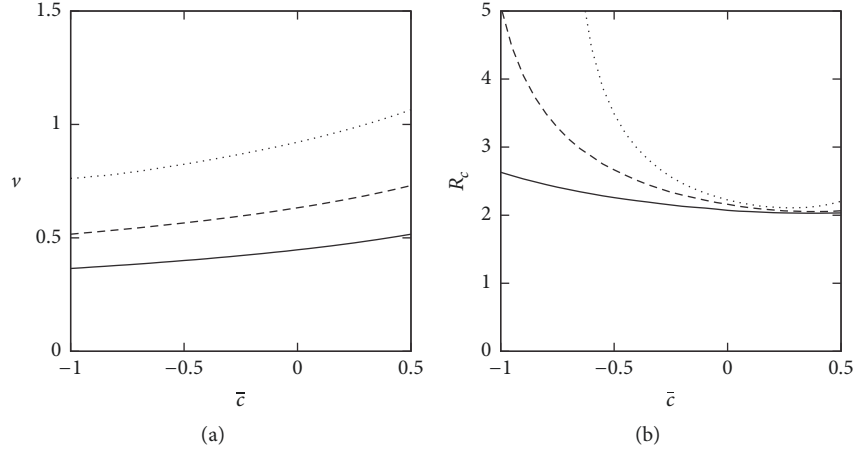
FIGURE 7: Dependence of velocity and radius on $\bar{c}$ in the stationary circular motion. Data are obtained by the simulation of the reduced tensor model. $\bar{b}_s = 0.1$. The solid, dashed, and dotted curves correspond to $(\gamma, \kappa) = (0.25, 0.1)$, $(0.5, 0.2)$, and $(1.0, 0.3)$, respectively. (a) Dependence of v on $\bar{c}$. (b) Dependence of R_c on $\bar{c}$.

decreases as the chemotaxis increases. When the condition $D_r = 0$ is satisfied, $v_{c,-} = v_{c,+}$ and $\Delta v_c^2 = 0$, which yields the critical value $\bar{c}^*$ as

$$\bar{c}^* = -\frac{\left(\overline{ab}\right)^2 + 4\kappa^2 \left(\overline{ab}_s\right)}{4\kappa \overline{ab}}. \tag{99}$$

When $|\bar{c}| > |\bar{c}^*|$, $D_r < 0$, and, therefore, $v_{c,\pm}^2$ does not exist. There is no parameter region of γ for a positive value of κ; the circular motion does not occur for any values of γ. The dependence of $\bar{c}^*$ on κ is shown in Figure 6(e). Equation (99) can be positive for large κ. However, when $\bar{c}$ is chosen as a positive value, the velocities v and s increase monotonically with increasing γ, and, therefore, the system diverges in the simulation. For this reason, $\bar{c}^*$ is shown in the range $\bar{c}^* \leq 0$.

In order to verify the above theoretical results, the simulation results for the reduced tensor model are shown in each figure. The results obtained via simulation agree well with the theoretical results. In Figures 6(a) and 6(b), for given κ and $\bar{c}$, there is only a lower limit of γ for the circular motion of the spot, resulting in v_c and $v_{c,+}$, respectively. On the other hand, in Figure 6(c), for given κ and $\bar{c}$, there is not only a lower limit of γ but also an upper limit of γ for the circular motion of the spot, resulting in $v_{c,+}$ and $v_{c,-}$, respectively. However, in Figure 6(e), for given κ and $\bar{c}^*$, there is no parameter region of γ for the circular motion of the spot.

The dependence of the stationary velocity and radius of the circular motion on $\bar{c}$ are shown in Figure 7. The velocity v increases monotonically with increasing $\bar{c}$, as shown in Figure 7(a). The corresponding radius of the spot motion R_c is shown in Figure 7(b). For fixed values of γ and κ, v decreases and R_c increases as $|\bar{c}|$ increases in the range $\bar{c} \leq 0$. The effect of chemotaxis is incorporated in $\bar{c}$, and $\bar{c}$ is negative; $|\bar{c}|$ increases as the intensity of chemotaxis k_c increases in our RD system (Figure 4(c)). Thus, it is seen that the chemotaxis reduces v and increases R_c.

From the above analyses on (85)–(88) with $\bar{b}_1 = 0$, we conclude four points on the properties of stationary circular motion. (i) There is a lower limit of velocity. (ii) Although there is no upper limit for the velocity when up to $O(\mathbf{v}^3)$ terms are considered, there will be an upper limit for the velocity if up to $O(\mathbf{v}^4)$ terms are considered. (iii) The range of velocity decreases as the chemotaxis increases. (iv) There is a critical value $\bar{c}^*$ (corresponding critical intensity of the chemotaxis is denoted by k_c^*) such that when $|\bar{c}| > |\bar{c}^*|$ ($k_c > k_c^*$), the circular motion does not occur for any values of γ.

6.4. Simulation of the Full Tensor Model.

In this subsection, we examine the effect of $U_{\alpha\beta\gamma}$ on v_α and $S_{\alpha\beta}$. For this, we consider the case of $\bar{b}_1 \neq 0$. The data are obtained by the simulation of the full tensor model.

The phase diagrams of the spot motion are shown in Figure 8. The phase diagrams in the $\bar{c}$-γ plane and $\bar{c}$-κ plane are shown in Figures 8(a) and 8(b), respectively. We note that the behaviors in the full tensor model are similar to that in the reduced model (Figures 5(b) and 5(c)). For positive (negative) $\bar{b}_1$, the region of the circular motion is larger (smaller). The phase diagrams in the $\bar{b}_1$-γ plane and $\bar{b}_1$-κ plane are shown in Figures 8(c) and 8(d), respectively. The behaviors are similar to the phase diagrams in the $\bar{c}$-γ plane and $\bar{c}$-κ plane. This result suggests that the effect of $\sum_\gamma U_{\alpha\beta\gamma} v_\gamma$ on the time evolution equation of $S_{\alpha\beta}$ is similar to that of $|\mathbf{v}|^2 S_{\alpha\beta}$.

The phase diagram of spot motion in the $\bar{c}$-$\bar{b}_1$ plane is shown in Figure 9. It can be seen that the circular motion occurs in the parameter region of positive and large values of $\bar{c}$ and $\bar{b}_1$. $S_{\alpha\beta}$ and $U_{\alpha\beta\gamma}$ measure the elliptical deformation and head-tail asymmetric deformation of the spot, respectively; these deformations lead to the circular motion.

The effects of $\bar{c}$ and $\bar{b}_1$ on the stationary velocity v and the corresponding radius of circular motion R_c are shown in Figure 10. On comparing these figures, it can
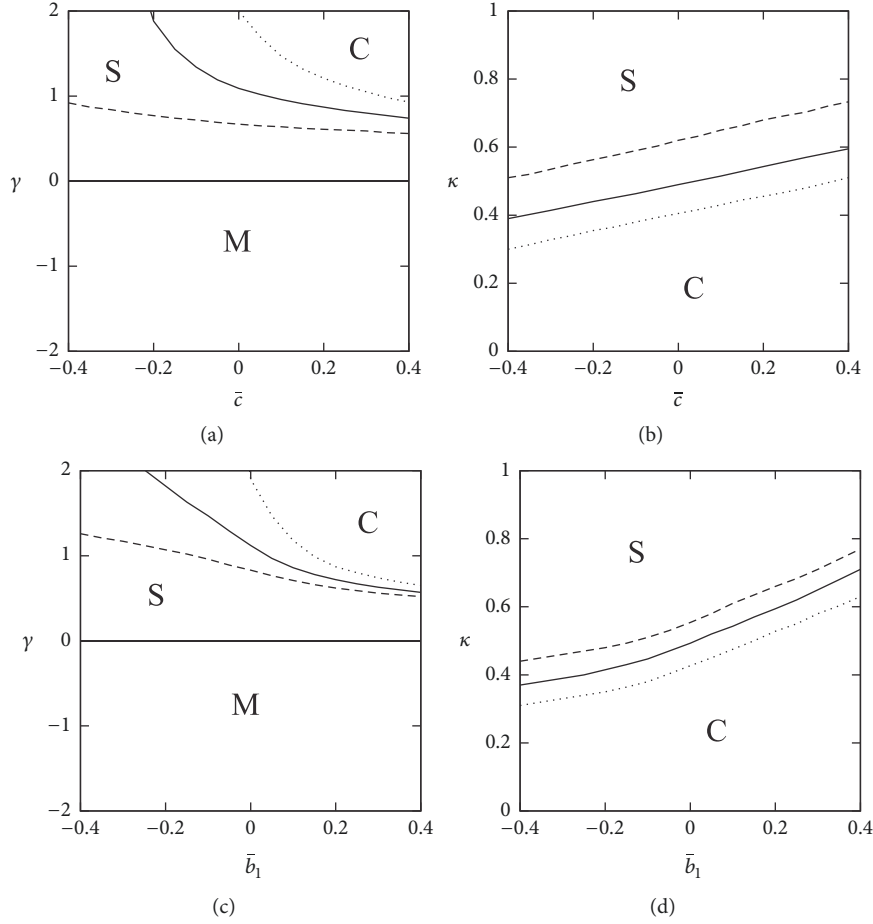
FIGURE 8: Phase diagram of spot motion. Data are obtained by the simulation of the full tensor model. $\bar{b}_s = 0.1$. M, S, and C in the figure represent regions of no motion, straight motion, and circular motion, respectively. (a) Phase diagram in the $\bar{c}$-γ plane. $\kappa = 0.8$. The solid, dashed, and dotted curves correspond to the cases of $\bar{b}_1 = 0, 0.25$, and -0.25, respectively. The upper (lower) region of each curve corresponds to the region of circular (straight) motion, and the region $\gamma \leq 0$ corresponds to the region of no motion. (b) Phase diagram in the $\bar{c}$-κ plane. $\gamma = 0.5$. The solid, dashed, and dotted curves correspond to the cases of $\bar{b}_1 = 0, 0.25$, and -0.25, respectively. The upper (lower) region of each curve corresponds to the region of straight (circular) motion. (c) Phase diagram in the $\bar{b}_1$-γ plane. $\kappa = 0.8$. The solid, dashed, and dotted curves correspond to the cases of $\bar{c} = 0, 0.25$, and -0.25, respectively. The region across each curve is the same as in (a). (d) Phase diagram in the $\bar{b}_1$-κ plane. $\gamma = 0.5$. The solid, dashed, and dotted curves correspond to the cases of $\bar{c} = 0, 0.25$, and -0.25, respectively. The region across each curve is the same as in (b).

be seen that although v and R_c depend on $\bar{c}$ and $\bar{b}_1$, the influences of $\bar{b}_1$ on v and R_c are much smaller than those of $\bar{c}$.

The dependence of the critical velocity $v_{c,\pm}$ and $\bar{c}^*$ on κ is shown in Figure 11. There exists a critical velocity $v_{c\pm}$ for $\bar{b}_1 \neq 0$ as shown in Figure 11(a). For larger $\bar{b}_1$, the gap Δv_c^2 is larger. This suggests that $\bar{b}_1 \sum_\gamma U_{\alpha\beta\gamma} v_\gamma$ enhances the circular motion, which is consistent with the results shown in Figure 8. For positive $\bar{b}_1$, $|\bar{c}^*|$ becomes larger than that in the reduced tensor model (solid curve) as shown in Figure 11(b). On the other hand, for negative $\bar{b}_1$, there is no $\bar{c}^*$. In our system, $\bar{b}_1$ is positive and increases as the intensity of chemotaxis k_c increases as shown in Figure 4(d). Thus, $\bar{c}^*$ still exists in the full tensor model, and $|\bar{c}^*|$ is larger than that in the reduced model.

7. Discussions

In this section, we discuss the physical origins of the braking effect observed in the previous section. For our RD system, we derived the time evolution equation of $S_{\alpha\beta}$ up to $O(\mathbf{v}^4)$ (see (77)). There were three terms of $O(\mathbf{v}^4)$: $\bar{b}_s(v_\alpha v_\beta - \delta_{\alpha\beta}|\mathbf{v}|^2/2)|\mathbf{v}|^2$, $\bar{b}_1 \sum_\gamma U_{\alpha\beta\gamma} v_\gamma$, and $\bar{c}|\mathbf{v}|^2 S_{\alpha\beta}$. The $\bar{b}_s$ term can be absorbed into the $\bar{b}(v_\alpha v_\beta - \delta_{\alpha\beta}|\mathbf{v}|^2/2)$ term by replacing $\bar{b}$ with $(\bar{b} + \bar{b}_s|\mathbf{v}|^2)$. Then, with increasing velocity, the $\bar{b}_s$ term changes the value of only $\bar{b}$. In our theoretical analysis, considering that the influence of $U_{\alpha\beta\gamma}$ is small, we set $\bar{b}_1 = 0$ and examined the effect of $\bar{c}|\mathbf{v}|^2 S_{\alpha\beta}$ on the stationary solution in Sections 6.2 and 6.3. When up to $O(\mathbf{v}^3)$ terms were considered, there was no upper limit of velocity for
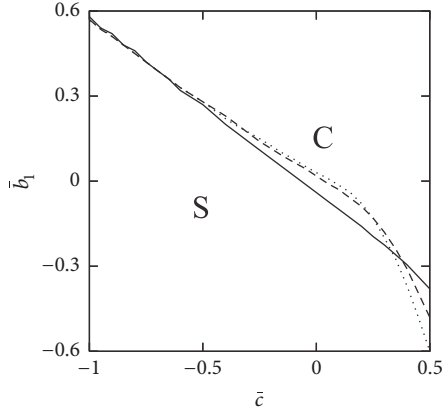
FIGURE 9: Phase diagram of spot motion in the $\bar{c}$-$\bar{b}_1$ plane. Data are obtained by the simulation of the full tensor model. $\bar{b}_s = 0.1$. The marks S and C in the figure represent regions of straight motion and circular motion, respectively. The solid, dashed, and dotted curves correspond to the cases of $(\gamma, \kappa) = (0.25, 0.3), (0.5, 0.5)$, and $(1.0, 0.8)$, respectively.

the circular motion of the spot, as shown in Figure 6(a). However, on including the $O(\mathbf{v}^4)$ terms, even in the absence of chemotaxis ($k_c = 0$), $\bar{c} \neq 0$. The term $\bar{c}|\mathbf{v}|^2 S_{\alpha\beta}$ influenced the upper limit of velocity of the circular motion, as shown in Figure 6(c). One of the physical origins of the upper limit of velocity is the refractory period behind the rear interface. When $k_c = 0$, the RD system described by (5) and (6) is considered to have an activator and an inhibitor, as reported by Krischer and Mikhailov [32]. When τ is large, the motionless pulse (localized domain) in one dimension is stable. With decreasing τ, the motionless pulse is destabilized into a traveling pulse in one dimension. For a traveling pulse in one dimension, there is a refractory period behind the rear interface. A repulsive interaction occurs between pulses in the wave train; the repulsion results from the refractory period imposed on the leading interface of a traveling pulse by the tail of the preceding pulse [38]. In two dimensions, when a spot moves along a circle, there is an upper limit of velocity due to the refractory period behind the rear interface; the refractory period causes a braking effect on the velocity of the spot traveling along a circle.

In the absence of chemotaxis, that is, $k_c = 0$, we estimate the upper limit of velocity. Let us consider the traveling pulse with velocity c in one dimension of the system described by (5) and (6) in the limit $\epsilon \rightarrow 0$. The spatial dependence of the inhibitor before the leading interface and that behind the rear interface are given by $v_{\text{lead}}(z) = C_{\text{lead}} \exp(\lambda_- z)$ ($z > 0$) and $v_{\text{rear}}(z) = C_{\text{rear}} \exp(\lambda_+ z)$ ($z < 0$), respectively, where $z = x - ct$, $\lambda_{\pm} = [-c \pm \sqrt{c^2 + 4\beta}]/2$, and $C_{\text{lead(rear)}}$ is a coefficient. Using these expressions, we estimate the relaxation length (refractory period) of the inhibitor behind the rear interface by the linear approximation of $1/\lambda_+ \sim c/\beta$ for large c. For the spot moving along a circle with a given radius r_0, the upper limit of velocity c_{max} will approximately satisfy the relation $2\pi r_0 \gg 1/\lambda_+ \sim c_{\text{max}}/\beta$: $c_{\text{max}} \ll 2\pi r_0 \beta$. This suggests that, for large c, the refractory period is proportional to c. As the

velocity of the spot increases, the inhibitor at the leading interfaces becomes large due to the overlap, and, therefore, the velocity becomes small (because of the first term in (16)). These effects on velocity are manifested when the spot moves rapidly along a circle with a small radius.

In the presence of chemotaxis, that is, $k_c > 0$, we discuss another physical origin of the braking effect. The chemotaxis is caused by the gradient of the chemotactic substance at the interface. In our RD system, the chemotactic substance is autosecretion; it is produced inside the spot and diffuses outward. The chemotactic substance is distributed around the center of the spot and monotonically decreases away from the center. For the traveling pulse, the chemotactic substance at the rear interface is larger than that at the leading interface. The gradient of the chemotactic substance at the leading (rear) interface is negative (positive). The absolute value of the gradient of the chemotactic substance at the leading interface is larger than that at the rear interface. In addition, $(d\chi/dv)$ at the leading and rear interfaces are positive. Overall, the chemotactic velocity is negative (because of the second term in (16)). Thus, the chemotaxis in our system essentially reduces velocity.

8. Conclusions

In this study, we considered the motion of a spot solution in two dimensions under the influence of chemotaxis. Starting from a three-component RD system, we proposed a two-component (an activator and a chemotactic substance) RD system with a global coupling term. We remark that, in our model system, the spot secretes the chemotactic substance from the inside and the motion of the spot is influenced by the chemotaxis. Thus, the model is an autonomous system. The chemotaxis term is of the Keller-Segel type, and the chemotactic velocity is opposite to the traveling direction. The reason for the opposite direction is that the system involves autosecretion, and the gradient of the chemotactic substance at the leading interface is negative. Although there have been several studies on the motion of spots under the influence of chemotaxis, the chemoattractant was supplied from the outside [20–23]. The spot in these models is driven toward the source (higher concentration) point of the chemoattractant. These models are nonautonomous systems, and, therefore, different from our model.

For the RD system, by employing the method proposed in [16], we derived the equation of motion of the spot and the time evolution equations of the tensors. Terms up to the fourth order of $\mathbf{v}$ were considered, and we found that the terms $|\mathbf{v}|^2 S_{\alpha\beta}$ and $\sum_{\gamma} U_{\alpha\beta\gamma} v_{\gamma}$ played an important role in the motion of the spot. Our numerical results suggested the existence of an upper limit of velocity for the circular motion of the spot due to the braking effect. There are two physical origins for the braking effect: the refractory period behind the rear interface and the chemotactic velocity opposite to the moving direction. The former is unique to the circular motion and is not applicable for a spot in straight motion. On the other hand, the latter is general in our autonomous chemotactic system and is applicable
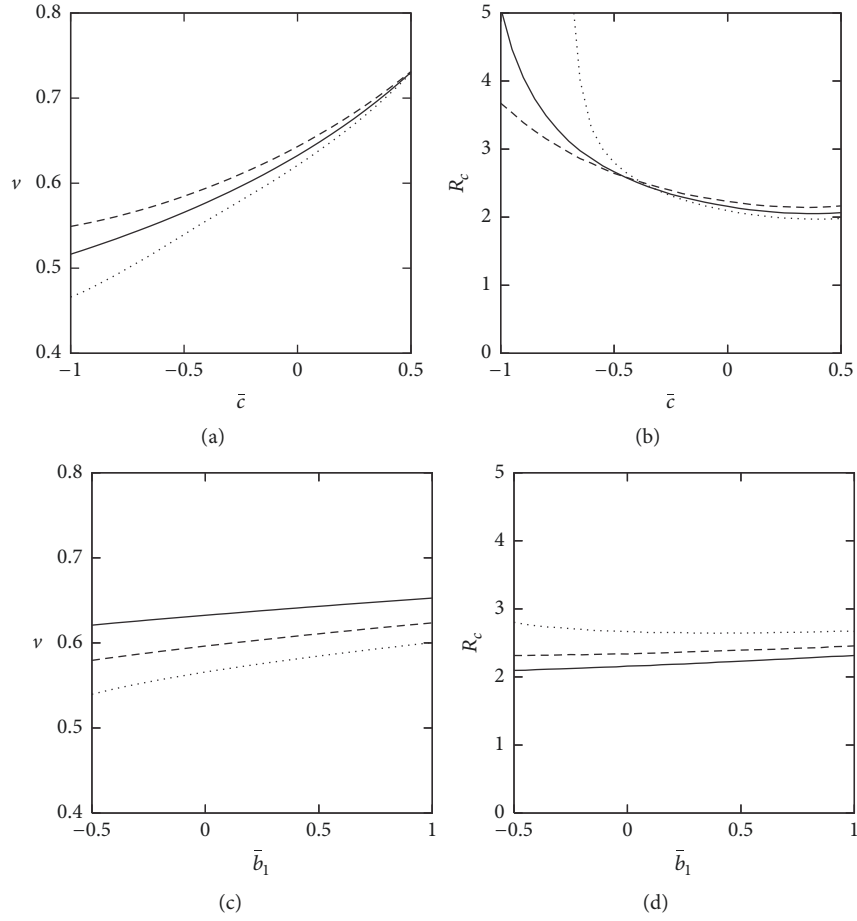
FIGURE 10: Dependence of velocity and radius on $\bar{c}$ and $\bar{b}_1$ in the stationary circular motion. Data are obtained by the simulation of the full tensor model. $\bar{b}_s = 0.1$, $\gamma = 0.5$, and $\kappa = 0.2$. (a) Dependence of v on $\bar{c}$. (b) Dependence of R_c on $\bar{c}$, where, in (a) and (b), the solid, dashed, and dotted curves correspo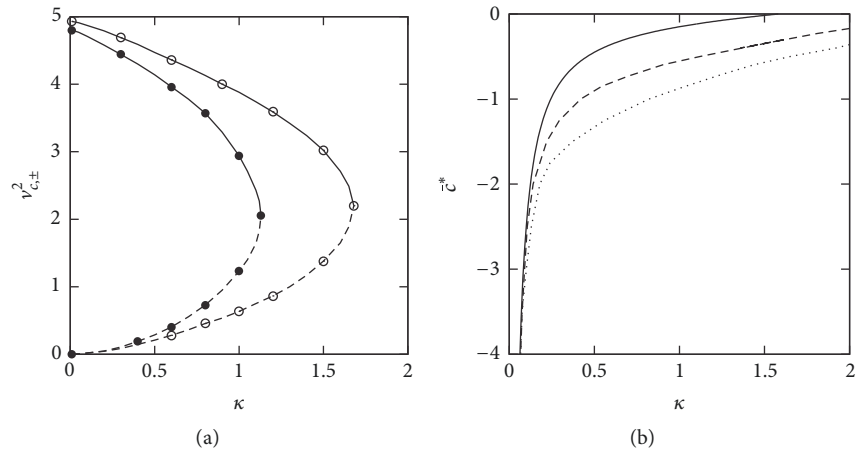nd to $\bar{b}_1 = 0$, 0.5, and −0.5, respectively. (c) Dependence of v on $\bar{b}_1$. (d) Dependence of R_c on $\bar{b}_1$, where, in (c) and (d), the solid, dashed, and dotted curves correspond to $\bar{c} = 0$, −0.25, and −0.5, respectively.

FIGURE 11: Dependence of the critical velocity $v_{c,\pm}$ and $\bar{c}^*$ on κ. Data are obtained by the simulation of the full tensor model. $\bar{b}_s = 0.1$. (a) Dependence of $v_{c,\pm}^2$ on κ. $\bar{c} = -0.5$. The curves with filled (•) and open (∘) circles correspond to the cases of $\bar{b}_1 = 0.25$ and $\bar{b}_1 = 0.5$, respectively. The solid and dashed curves represent $v_{c,-}^2$ and $v_{c,+}^2$, respectively. (b) Dependence of $\bar{c}^*$ on κ. $\bar{b}_s = 0.1$. The solid, dashed, and dotted curves correspond to the cases of $\bar{b}_1 = 0$, 0.25, and 0.5, respectively.

for all moving directions. Owing to the former reason, an upper limit of velocity for the spot moving in a circle exists even in the absence of chemotaxis. Based on the results of our chemotaxis system, we conclude three points. (i) A spot moving on a straight line is destabilized to circular motion with increasing velocity. (ii) The velocity of a spot moving along a circle is restricted to a certain range, which is narrower than that in the absence of the chemotaxis. (iii) There is a critical intensity of chemotaxis k_c^*, and the spot does not undergo circular motion for $k_c > k_c^*$.

In practical experiments, the candidates of autonomous systems including chemotaxis are *E. coli* and macrophage [39, 40]. However, there is an essential difference between these biological systems and our model system; *E. coli* is a rod-shaped cell with a flagellum and macrophage has an amoeba-like shape with pseudopods, and the shape of the motionless state of these cells is not described by a circle. *E. coli* swims by rotating the flagellum, and macrophage crawls by changing its size and shape. In contrast, in our model system, the spot was a solution of an RD system and the shape of the motionless state was assumed to be a circle. The motionless spot was primarily destabilized through drift bifurcation, and it changed into a moving spot with straight motion. The straight moving spot was secondly destabilized through rotation bifurcation, and it changed into a moving spot with circular motion. Due to these differences, the bifurcation points of the straight and circular motions and the critical velocity for the circular motion in these biological systems must be different from those of our model system. However, the collective motions of bacteria and amoebas are modeled by RD systems, and many spatiotemporal patterns are shown [41, 42]: the diffusion-limited aggregation, Eden-like, uniform disk, branched, target, spiral patterns, and so on. This suggests that the behavior of individual cell in these biological systems can be described by RD systems. From these considerations, the above biological systems are promising candidates of autonomous systems including chemotaxis, and experimental observations of moving cell with circular motion are expected.

Appendix

A. Velocity of the Interface in One Dimension

Here, we derive the velocity of the interface in one dimension, given by (16), by following [43]. We denote h as the value of v at the interface $x = x_0$ at time $t = t_0$. Applying the stretching transformations $\eta = (t - t_0)/\epsilon$ and $\xi = (x - x_0)/\epsilon$ to (5), we obtain

$$
\tau u_\eta = u_{\xi\xi} - \left(\frac{d\chi}{dv} \right)\bigg|_i \left(\frac{dv}{dx} \right)\bigg|_i u_\xi - u
$$
$$
+ H(u - p) - h,
$$
(A.1)

where $(A)|_i$ denotes the function A evaluated at $x = x_0$, and the position of the interface in the stretching coordinate is $\xi = 0$. In order to consider the traveling front solution of (A.1),

we introduce the moving coordinate $z = \xi - c\eta$. Then, (A.1) becomes

$$
\tau u_\eta = u_{zz} + \left(\tau c - \left(\frac{d\chi}{dv} \right)\bigg|_i \left(\frac{dv}{dx} \right)\bigg|_i \right) u_z - u
$$
$$
+ H(u - p) - h
$$
(A.2)
$$
\equiv u_{zz} + c' u_z - u + H(u - p) - h,
$$

where c is the velocity of the front and $c' = (\tau c - (d\chi/dv)|_i (dv/dx)|_i)$. The boundary conditions at $z = \pm\infty$ are

$$
u(-\infty, \eta) = 1 - h,
$$
$$
u(+\infty, \eta) = -h,
$$
(A.3)

and the boundary conditions at $z = 0$ are

$$
u(0+, \eta) = u(0-, \eta) = p,
$$
$$
u_z(0+, \eta) = u_z(0-, \eta).
$$
(A.4)

The stationary solution of (A.2) is

$$
u(z) = \begin{cases} C_- e^{\lambda_+ z} + (1 - h) & (z < 0), \\ C_+ e^{\lambda_- z} - h & (z \geq 0), \end{cases}
$$
(A.5)

where $C_\pm$ is a coefficient and $\lambda_\pm = (1/2)[-c' \pm \sqrt{c'^2 + 4}]$. Under the boundary conditions (A.4), we get $C_+ = \lambda_+/(\lambda_+ - \lambda_-) = p + h$ and $C_- = \lambda_-/(\lambda_+ - \lambda_-) = p + h - 1$. Using these relations, we obtain

$$
c' = \tau c - \left(\frac{d\chi}{dv} \right)\bigg|_i \left(\frac{dv}{dx} \right)\bigg|_i
$$
$$
= \frac{2(1/2 - p - h)}{[(p + h)(1 - p - h)]^{1/2}}.
$$
(A.6)

In the main text, τc in (A.6) is denoted as $\tau C(h)$, which is explicitly expressed as (16).

B. Explicit Expressions of $h_0^{(0)}$ and $\widetilde{h}_0^{(0)}$ in the Limit $\epsilon \to 0$

We show that in the limit $\epsilon \to 0$, $h_0^{(0)}$ and $\widetilde{h}_0^{(0)}$ calculated using (13) agree with the ones calculated using (34) and (35) with the substitutions $H_q = H_q^{(0)}$ and $\mathbf{R} = \mathbf{R}^{(0)}$, where $\mathbf{R}^{(0)} = R_0 \mathbf{e}_r$, respectively.

$h_0^{(0)}$ and $\widetilde{h}_0^{(0)}$ obtained directly from (13) are

$$
h_0^{(0)} = \bar{v}(R_0) = \frac{1}{\beta} - \frac{R_0}{\sqrt{\beta}} K_1\left(\sqrt{\beta} R_0 \right) I_0\left(\sqrt{\beta} R_0 \right), \quad (B.1)
$$

$$\tilde{h}_0^{(0)} = \frac{d\bar{v}(R_0)}{dr} = -R_0 I_1\left(\sqrt{\beta}R_0\right) K_1\left(\sqrt{\beta}R_0\right), \tag{B.2}$$

respectively.

We first derive $h_0^{(0)}$ from the definition (34). Substituting $H_\mathbf{q} = H_\mathbf{q}^{(0)}$ and $\mathbf{R} = \mathbf{R}^{(0)}$ into (34), we obtain

$$\begin{aligned} h_0^{(0)} &= \int_\mathbf{q} G_q H_\mathbf{q}^{(0)} e^{i\mathbf{q}\cdot\mathbf{R}^{(0)}} \\ &= R_0 \int_0^\infty dq\left(\frac{1}{q^2+\beta}\right) J_0\left(qR_0\right) J_1\left(qR_0\right). \end{aligned} \tag{B.3}$$

We apply the formulas of the integrals ([44])

$$\begin{aligned} &\int_0^\infty dx \frac{x^{\mu+1}}{\left(x^2+t^2\right)\left(x^2+y^2\right)^{\nu/2}} J_\nu\left(a\sqrt{x^2+y^2}\right) J_\mu\left(bx\right) \\ &= \frac{t^\mu J_\nu\left(a\sqrt{y^2-t^2}\right)}{\left(y^2-t^2\right)^{\nu/2}} K_\mu\left(bt\right) \end{aligned} \tag{B.4}$$

$$\left(b \ge a > 0, \ \left|\mathrm{Re}\left(\mu\right)\right| < \mathrm{Re}\left(\nu\right)+2\right),$$

$$\int_0^\infty dx J_0\left(ax\right) J_1\left(bx\right) = \begin{cases} \dfrac{1}{b} & (b > a > 0), \\ \dfrac{1}{2b} & (b = a > 0), \\ 0 & (a > b > 0) \end{cases} \tag{B.5}$$

to (B.3); we can confirm that (B.3) agrees with (B.1).

Next, we derive $\tilde{h}_0^{(0)}$ from the definition (35). Substituting $H_\mathbf{q} = H_\mathbf{q}^{(0)}$ and $\mathbf{R} = \mathbf{R}^{(0)}$ into (35), we obtain

$$\begin{aligned} \tilde{h}_0^{(0)} &= i\int_\mathbf{q} \left(\mathbf{n}\cdot\mathbf{q}\right) G_q H_\mathbf{q}^{(0)} e^{i\mathbf{q}\cdot\mathbf{R}^{(0)}} \\ &= -R_0 \int_0^\infty dq\left(\frac{q}{q^2+\beta}\right) J_1^2\left(qR_0\right). \end{aligned} \tag{B.6}$$

Applying formula (B.4) to (B.6), we can confirm that (B.6) agrees with (B.2).

C. Derivation of (68)

Here, we give the detailed derivation of (68). We first derive $\delta\mathbf{h}_{1,1}^{(0)}$. Up to the first order of the deviations, $\delta\mathbf{h}_{1,1}^{(0)}$ is decomposed as

$$\begin{aligned} \delta\mathbf{h}_{1,1}^{(0)} &= \frac{i}{\Omega} \int_\mathbf{q} \int d\omega\left(\mathbf{v}\cdot\mathbf{q}\right) G_q^2 H_\mathbf{q} e^{i\mathbf{q}\cdot\mathbf{R}}\mathbf{R} \\ &\quad -\frac{i}{\Omega} \int_\mathbf{q} \int d\omega\left(\mathbf{v}\cdot\mathbf{q}\right) G_q^2 H_\mathbf{q}^{(0)} e^{i\mathbf{q}\cdot\mathbf{R}_0}\mathbf{R}_0 \\ &\quad \sim \frac{i}{\Omega} \int_\mathbf{q} \int d\phi_r\left(\mathbf{v}\cdot\mathbf{q}\right) G_q^2 H_\mathbf{q}^{(1)} e^{i\mathbf{q}\cdot\mathbf{R}_0} R_0^2 \mathbf{e}_r \\ &\quad -\frac{1}{\Omega} \int_\mathbf{q} \int d\phi_r\left(\mathbf{v}\cdot\mathbf{q}\right)\left(\mathbf{q}\cdot\delta\mathbf{R}\left(\phi_r\right)\right) \\ &\quad \times G_q^2 H_\mathbf{q}^{(0)} e^{i\mathbf{q}\cdot\mathbf{R}_0} R_0^2 \mathbf{e}_r \\ &\quad +\frac{2i}{\Omega} \int_\mathbf{q} \int d\phi_r\left(\mathbf{v}\cdot\mathbf{q}\right) G_q^2 H_\mathbf{q}^{(0)} e^{i\mathbf{q}\cdot\mathbf{R}_0} \delta R\left(\phi_r\right) R_0 \mathbf{e}_r \\ &\quad \equiv \mathbf{\Phi}_1 + \mathbf{\Phi}_2 + \mathbf{\Phi}_3, \end{aligned} \tag{C.1}$$

where δR and $H_\mathbf{q}$ are given in (25) and (31), respectively.

Substituting $H_\mathbf{q}^{(1)}$ into $\mathbf{\Phi}_1$, the α ($\alpha = 1, 2$) component $\Phi_{1(\alpha)}$ is obtained as

$$\Phi_{1(\alpha)} = \frac{R_0}{2} \int dq q^2 G_q^2 J_1 J_2 \sum_\beta S_{\alpha\beta} v_\beta \equiv -a_1^* \sum_\beta S_{\alpha\beta} v_\beta. \tag{C.2}$$

Substituting $\delta\mathbf{R}(\phi_r)$ and $H_\mathbf{q}^{(0)}$ into $\mathbf{\Phi}_2$, $\Phi_{2(\alpha)}$ is obtained as

$$\Phi_{2(\alpha)} = \left[\frac{R_0}{4} \int dq q^2 G_q^2 J_1 J_2 - \frac{R_0}{4} \int dq q^2 G_q^2 J_0 J_1\right] \sum_\beta S_{\alpha\beta} v_\beta. \tag{C.3}$$

Substituting $\delta\mathbf{R}(\phi_r)$ and $H_\mathbf{q}^{(0)}$ into $\mathbf{\Phi}_3$, $\Phi_{3(\alpha)}$ is obtained as

$$\Phi_{3(\alpha)} = -\int dq q G_q^2 J_1^2 \sum_\beta S_{\alpha\beta} v_\beta. \tag{C.4}$$

Using the formula for the Bessel function $(J_{n-1}(z) - J_{n+1}(z))/2 = J_{n+1}(z) - nJ_n(z)/z$, $(\Phi_{2(\alpha)} + \Phi_{3(\alpha)})$ becomes

$$\begin{aligned} &\left(\Phi_{2(\alpha)} + \Phi_{3(\alpha)}\right) \\ &= \left[\frac{R_0}{2} \int dq q^2 G_q^2 J_1 J_2 - \frac{3}{2} \int dq q G_q^2 J_1^2\right] \sum_\beta S_{\alpha\beta} v_\beta \\ &\equiv -a_2^* \sum_\beta S_{\alpha\beta} v_\beta. \end{aligned} \tag{C.5}$$

a_1^* and a_2^* are the same as those of the result in [16].

Next, we derive $\delta\widetilde{\mathbf{h}}_{1,1}^{(0)}$. Up to the first order of the deviations, $\delta\widetilde{\mathbf{h}}_{1,1}^{(0)}$ is decomposed as

$$
\begin{aligned}
\delta\widetilde{\mathbf{h}}_{1,1}^{(0)} &= \frac{-1}{\Omega} \int_{\mathbf{q}} \int d\omega \, (\mathbf{n} \cdot \mathbf{q})(\mathbf{v} \cdot \mathbf{q}) \, G_q^2 H_{\mathbf{q}} e^{i\mathbf{q}\cdot\mathbf{R}} \mathbf{R} \\
&+ \frac{1}{\Omega} \int_{\mathbf{q}} \int d\omega \, (\mathbf{n} \cdot \mathbf{q})(\mathbf{v} \cdot \mathbf{q}) \, G_q^2 H_{\mathbf{q}}^{(0)} e^{i\mathbf{q}\cdot\mathbf{R}_0} \mathbf{R}_0 \\
&\sim \frac{-2}{\Omega} \int_{\mathbf{q}} \int d\phi_r \, (\mathbf{n} \cdot \mathbf{q})(\mathbf{v} \cdot \mathbf{q}) \, G_q^2 H_{\mathbf{q}}^{(0)} e^{i\mathbf{q}\cdot\mathbf{R}_0} R_0 \delta R(\phi_r) \mathbf{e}_r \\
&- \frac{1}{\Omega} \int_{\mathbf{q}} \int d\phi_r \, (\mathbf{n} \cdot \mathbf{q})(\mathbf{v} \cdot \mathbf{q}) \, G_q^2 H_{\mathbf{q}}^{(1)} e^{i\mathbf{q}\cdot\mathbf{R}_0} R_0^2 \mathbf{e}_r \\
&- \frac{1}{\Omega} \int_{\mathbf{q}} \int d\phi_r \, (\mathbf{n} \cdot \mathbf{q})(\mathbf{v} \cdot \mathbf{q})(i\mathbf{q} \cdot \delta\mathbf{R}(\phi_r)) \\
&\times G_q^2 H_{\mathbf{q}}^{(0)} e^{i\mathbf{q}\cdot\mathbf{R}_0} R_0^2 \mathbf{e}_r \\
&+ \frac{1}{\Omega} \int_{\mathbf{q}} \int d\phi_r \, (\mathbf{v} \cdot \mathbf{q}) q \delta R'(\phi_r) \sin(\phi_q - \phi_r) \\
&\times G_q^2 H_{\mathbf{q}}^{(0)} e^{i\mathbf{q}\cdot\mathbf{R}_0} R_0 \mathbf{e}_r \\
&\equiv \mathbf{\Psi}_1 + \mathbf{\Psi}_2 + \mathbf{\Psi}_3 + \mathbf{\Psi}_4.
\end{aligned}
\tag{C.6}
$$

Substituting $H_{\mathbf{q}}^{(0)}$ and $\delta R(\phi_r)$ into $\mathbf{\Psi}_1$, the α ($\alpha = 1, 2$) component $\Psi_{1(\alpha)}$ is obtained as

$$
\Psi_{1(\alpha)} = \int dq q G_q^2 (J_2 - J_0) J_1 \sum_\beta S_{\alpha\beta} v_\beta.
\tag{C.7}
$$

Substituting $H_{\mathbf{q}}^{(1)}$ into $\mathbf{\Psi}_2$, $\Psi_{2(\alpha)}$ is obtained as

$$
\Psi_{2(\alpha)} = -\frac{R_0}{4} \int dq q^2 G_q^2 (J_2 - J_0) J_2 \sum_\beta S_{\alpha\beta} v_\beta.
\tag{C.8}
$$

Substituting $H_{\mathbf{q}}^{(0)}$ and $\delta\mathbf{R}$ into $\mathbf{\Psi}_3$, $\Psi_{3(\alpha)}$ is obtained as

$$
\Psi_{3(\alpha)} = \frac{R_0}{8} \int dq q^3 G_q^2 (3J_1 - J_2) J_1 \sum_\beta S_{\alpha\beta} v_\beta.
\tag{C.9}
$$

Substituting $H_{\mathbf{q}}^{(0)}$ and $\delta R'(\phi_r)$ into $\mathbf{\Psi}_4$, $\Psi_{4(\alpha)}$ is obtained as

$$
\Psi_{4(\alpha)} = \frac{3}{4} \int dq q^2 G_q^2 J_0 J_1 \sum_\beta S_{\alpha\beta} v_\beta.
\tag{C.10}
$$

In the main text, $(\Psi_{3(\alpha)} + \Psi_{4(\alpha)})$ is expressed as

$$
\begin{aligned}
&(\Psi_{3(\alpha)} + \Psi_{4(\alpha)}) \\
&= \int dq q^2 G_q^2 \left[\frac{R_0}{8} q (3J_1 - J_2) J_1 + \frac{3}{4} J_0 J_1 \right] \sum_\beta S_{\alpha\beta} v_\beta \\
&\equiv -\widetilde{a}_1^* \sum_\beta S_{\alpha\beta} v_\beta,
\end{aligned}
\tag{C.11}
$$

and $(\Psi_{1(\alpha)} + \Psi_{2(\alpha)})$ is expressed as

$$
\begin{aligned}
&(\Psi_{1(\alpha)} + \Psi_{2(\alpha)}) \\
&= 2 \int dq q G_q^2 \left[\frac{1}{4} R_0 q J_2 - J_1 \right] \frac{\partial J_1}{\partial(qR_0)} \sum_\beta S_{\alpha\beta} v_\beta \\
&\equiv -\widetilde{a}_2^* \sum_\beta S_{\alpha\beta} v_\beta,
\end{aligned}
\tag{C.12}
$$

where we used $J_n'(z) = (J_{n-1} - J_{n+1})/2$ as the formula for the Bessel function.

D. Expansions of δh and $\delta\widetilde{h}$ in (75) and (76)

The expansions of δh and $\delta\widetilde{h}$ in (75) and (76) are

$$
\delta h_0 = -\sum_n D_n c_n e^{in\phi_r},
$$

$$
\delta h_{1,1} = -\frac{v_-}{2} \sum_n A_n c_n e^{i(n+1)\phi_r} - \frac{v_+}{2} \sum_n B_n c_n e^{i(n-1)\phi_r},
$$

$$
\delta h_{1,2} = -\sum_n E_n \dot{c}_n e^{in\phi_r},
$$

$$
\begin{aligned}
\delta h_{2,2} &= -\frac{G_0}{2} |\mathbf{v}|^2 + \frac{G_1}{4} \left(v_-^2 e^{2i\phi_r} + v_+^2 e^{-2i\phi_r} \right) \\
&+ \sum_n c_n e^{in\phi_r} \left[v_-^2 e^{2i\phi_r} T_{n,1} - 2 |\mathbf{v}|^2 T_{n,2} + v_+^2 e^{-2i\phi_r} T_{n,3} \right] \\
&+ \sum_n c_n e^{in\phi_r} \left[\left(v_-^2 e^{2i\phi_r} + v_+^2 e^{-2i\phi_r} \right) V_1 + |\mathbf{v}|^2 V_2 \right],
\end{aligned}
\tag{D.1}
$$

$$
\cdots = \cdots,
$$

$$
\delta\widetilde{h}_0 = -\sum_n \widetilde{D}_n c_n e^{in\phi_r},
$$

$$
\begin{aligned}
\delta\widetilde{h}_{1,1} &= -\frac{v_-}{2} \sum_n \left(\widetilde{A}_n + n\widetilde{A}^* \right) c_n e^{i(n+1)\phi_r} \\
&- \frac{v_+}{2} \sum_n \left(\widetilde{B}_n - n\widetilde{A}^* \right) c_n e^{i(n-1)\phi_r},
\end{aligned}
$$

$$
\delta\widetilde{h}_{1,2} = -\sum_n \widetilde{E}_n \dot{c}_n e^{in\phi_r},
$$

$$
\begin{aligned}
\delta\widetilde{h}_{2,2} &= \sum_n \widetilde{S}^* c_n n \left(v_+^2 e^{-2i\phi_r} - v_-^2 e^{2i\phi_r} \right) e^{in\phi_r} \\
&+ \left[-\frac{\widetilde{G}_0}{2} |\mathbf{v}|^2 + \frac{\widetilde{G}_1}{4} \left(v_-^2 e^{2i\phi_r} + v_+^2 e^{-2i\phi_r} \right) \right] \\
&+ \sum_n c_n e^{in\phi_r} \left[v_-^2 e^{2i\phi_r} \widetilde{T}_{n,1} - 2 |\mathbf{v}|^2 \widetilde{T}_{n,2} + v_+^2 e^{-2i\phi_r} \widetilde{T}_{n,3} \right] \\
&+ \sum_n c_n e^{in\phi_r} \left[\left(v_-^2 e^{2i\phi_r} + v_+^2 e^{-2i\phi_r} \right) \widetilde{V}_1 + |\mathbf{v}|^2 \widetilde{V}_2 \right],
\end{aligned}
\tag{D.2}
$$

$$
\cdots = \cdots,
$$

where $v_\pm = v_1 \pm iv_2$ and all the coefficients in (D.1) and (D.2) are given in Appendix E. In order to calculate the time

evolution of c_n, $e^{-in\phi_r}$ is multiplied to both sides of eq. (74), and integration is performed over ϕ_r in the range $0 \leq \phi_r \leq 2\pi$. Using the periodicity of trigonometric functions, we obtain the time evolution equation of c_n. As the tensors $\mathbf{S}$ and $\mathbf{U}$ are linear combinations of $c_{\pm n}$, we can derive their time evolution equations.

E. Coefficients in (D.1) and (D.2)

We give the coefficients in (D.1) and (D.2) below. By using $F(i, j, k, l)$ and $F_d(i, j, k, l)$, they are expressed as

$$A_n = R_0 \left[F(2, 2, n, n+1) + F_d(2, 2, 1, 1) \right],$$

$$B_n = R_0 \left[-F(2, 2, n, n-1) + F_d(2, 2, 1, 1) \right],$$

$$D_n = R_0 \left[F(1, 1, 1, 1) - F(1, 1, n, n) \right],$$

$$E_n = R_0 F(1, 2, n, n),$$

$$G_n = R_0 F(2, 3, n, n+1),$$

$$G_1^s = R_0 F(4, 5, 1, 2),$$

$$T_{n,1} = \frac{R_0}{4} F(3, 3, n, n+2),$$

$$T_{n,2} = \frac{R_0}{4} F(3, 3, n, n),$$

$$T_{n,3} = \frac{R_0}{4} F(3, 3, n, n-2),$$

$$V_1 = \frac{R_0}{4} F_d(3, 3, 1, 2),$$

$$V_2 = \frac{R_0}{2} F(3, 3, 1, 1),$$

$$\widetilde{A}_n = R_0 \left[\frac{1}{4} \left(F(3, 2, 1, 3) - 3F(3, 2, 1, 1) \right) \right.$$
$$\left. + F_d(3, 2, n, n+1) \right],$$

$$\widetilde{A}^* = \frac{1}{2} \left[F(2, 2, 0, 1) + F(2, 2, 1, 2) \right],$$

$$\widetilde{B}_n = R_0 \left[\frac{1}{4} \left(F(3, 2, 1, 3) - 3F(3, 2, 1, 1) \right) \right.$$
$$\left. - F_d(3, 2, n, n-1) \right],$$

$$\widetilde{D}_n = R_0 \left[F_d(2, 1, 1, 1) - F_d(2, 1, n, n) \right],$$

$$\widetilde{E}_n = R_0 F_d(2, 2, n, n),$$

$$\widetilde{G}_0 = R_0 F_d(3, 3, 1, 0),$$

$$\widetilde{G}_1 = R_0 F_d(3, 3, 1, 2),$$

$$\widetilde{G}_1^s = R_0 F_d(5, 5, 1, 2),$$

$$\widetilde{S}^* = -\frac{1}{8} \left[F(3, 3, 1, 1) + F(3, 3, 1, 3) \right],$$

(E.1)

$$\widetilde{T}_{n,1} = \frac{R_0}{4} F_d(4, 3, n, n+2),$$

$$\widetilde{T}_{n,2} = \frac{R_0}{4} F_d(4, 3, n, n),$$

$$\widetilde{T}_{n,3} = \frac{R_0}{4} F_d(4, 3, n, n-2),$$

$$\widetilde{V}_1 = \frac{R_0}{16} \left[F(4, 3, 0, 1) - 2F(4, 3, 1, 2) + F(4, 3, 1, 4) \right],$$

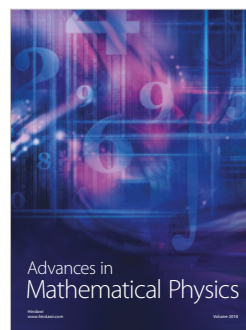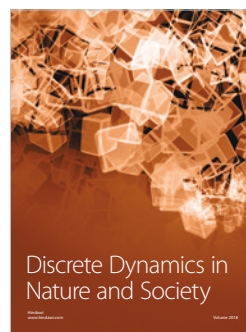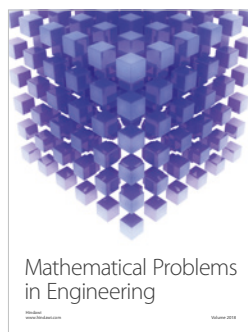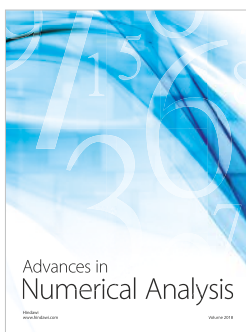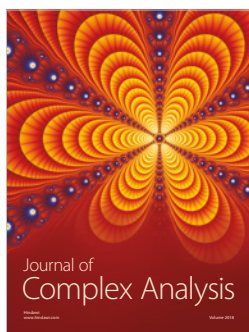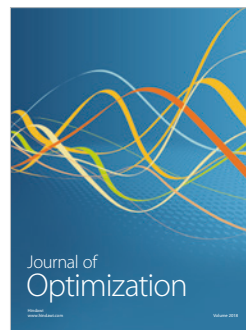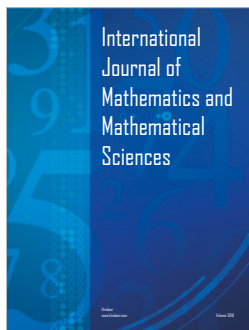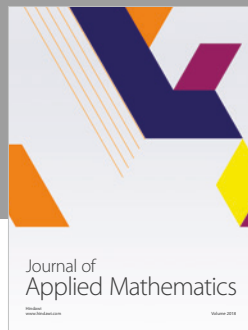$$\widetilde{V}_2 = \frac{R_0}{2} F_d(4, 3, 1, 1).$$

(E.2)

Conflicts of Interest

The author declares that there are no conflicts of interest.

References

[1] J. Elgeti, R. G. Winkler, and G. Gompper, "Physics of micro-swimmers-single particle motion and collective behavior: a review," *Reports on Progress in Physics*, vol. 78, no. 5, Article ID 056601, 2015.

[2] K. Kroy, D. Chakraborty, and F. Cichos, "Hot microswimmers," *The European Physical Journal Special Topics*, vol. 225, no. 11-12, pp. 2207–2225, 2016.

[3] A. Geiseler, P. Hänggi, and F. Marchesoni, "Self-Polarizing Microswimmers in Active Density Waves," *Scientific Reports*, vol. 7, Article ID 41884, 2017.

[4] Y.-J. Chen and K. Yoshikawa, "Interface dynamics under nonequilibrium conditions: From a self-propelled droplet to dynamic pattern evolution," *European Physical Journal E*, vol. 34, no. 4, Article ID i2011-11038-3, 2011.

[5] N. Yoshinaga, K. H. Nagai, Y. Sumino, and H. Kitahata, "Drift instability in the motion of a fluid droplet with a chemically reactive surface driven by Marangoni flow," *Physical Review E: Statistical, Nonlinear, and Soft Matter Physics*, vol. 86, no. 1, Article ID 016108, 2012.

[6] S. Yabunaka, T. Ohta, and N. Yoshinaga, "Self-propelled motion of a fluid droplet under chemical reaction," *The Journal of Chemical Physics*, vol. 136, no. 7, Article ID 074904, 2012.

[7] M. Tarama, A. M. Menzel, B. Ten Hagen, R. Wittkowski, T. Ohta, and H. Löwen, "Dynamics of a deformable active particle under shear flow," *The Journal of Chemical Physics*, vol. 139, no. 10, Article ID 104906, 2013.

[8] M. Tarama, A. M. Menzel, and H. Löwen, "Deformable microswimmer in a swirl: Capturing and scattering dynamics," *Physical Review E: Statistical, Nonlinear, and Soft Matter Physics*, vol. 90, no. 3, Article ID 032907, 2014.

[9] Y.-J. Chen, Y. Nagamine, and K. Yoshikawa, "Self-propelled motion of a droplet induced by Marangoni-driven spreading," *Physical Review E: Statistical, Nonlinear, and Soft Matter Physics*, vol. 80, no. 1, Article ID 016303, 2009.

[10] S. Thutupalli, R. Seemann, and S. Herminghaus, "Swarming behavior of simple model squirmers," *New Journal of Physics*, vol. 13, Article ID 073021, 2011.

[11] K. H. Nagai, F. Takabatake, Y. Sumino, H. Kitahata, M. Ichikawa, and N. Yoshinaga, "Rotational motion of a droplet induced by interfacial tension," *Physical Review E: Statistical, Nonlinear, and Soft Matter Physics*, vol. 87, no. 1, Article ID 013009, 2013.

[12] S. Tanaka, Y. Sogabe, and S. Nakata, "Spontaneous change in trajectory patterns of a self-propelled oil droplet at the air-surfactant solution interface," *Physical Review E: Statistical, Nonlinear, and Soft Matter Physics*, vol. 91, no. 3, Article ID 032406, 2015.

[13] M. Tarama, Y. Itino, A. M. Menzel, and T. Ohta, "Individual and collective dynamics of self-propelled soft particles," *The European Physical Journal Special Topics*, vol. 223, no. 1, pp. 121–139, 2014.

[14] T. Ohta, "Dynamics of deformable active particles," *Journal of the Physical Society of Japan*, vol. 86, no. 7, Article ID 072001, 2017.

[15] T. Ohta, "Pulse dynamics in a reaction-diffusion system," *Physica D: Nonlinear Phenomena*, vol. 151, no. 1, pp. 61–72, 2001.

[16] T. Ohta, T. Ohkuma, and K. Shitara, "Deformation of a self-propelled domain in an excitable reaction-diffusion system," *Physical Review E: Statistical, Nonlinear, and Soft Matter Physics*, vol. 80, no. 5, Article ID 056203, 2009.

[17] K. Shitara, T. Hiraiwa, and T. Ohta, "Deformable self-propelled domain in an excitable reaction-diffusion system in three dimensions," *Physical Review E: Statistical, Nonlinear, and Soft Matter Physics*, vol. 83, no. 6, Article ID 066208, 2011.

[18] A. Nishikimi, H. Fukuhara, W. Su et al., "Sequential regulation of DOCK2 dynamics by two phospholipids during neutrophil chemotaxis," *Science*, vol. 324, no. 5925, pp. 384–387, 2009.

[19] E. F. Keller and L. A. Segel, "Initiation of slime mold aggregation viewed as an instability," *Journal of Theoretical Biology*, vol. 26, no. 3, pp. 399–415, 1970.

[20] J. Song and D. Kim, "Three-dimensional chemotaxis model for a crawling neutrophil," *Physical Review E: Statistical, Nonlinear, and Soft Matter Physics*, vol. 82, no. 5, Article ID 051902, 2010.

[21] J. Song and D. Kim, "Computational kinetic study of chemotactic cell migration," *Journal of Applied Physics*, vol. 114, no. 15, Article ID 154701, 2013.

[22] L. Zhang, J. Song, and D. Kim, "A study on the interfacial effect on cancer-cell invasion," *Journal of Applied Physics*, vol. 109, no. 7, Article ID 074702, 2011.

[23] L. Zhang, S. Kang, and D. Kim, "Computational analysis of the effects of matrix-degrading enzymes on cancer-cell invasion," *Journal of Applied Physics*, vol. 112, no. 12, Article ID 124704, 2012.

[24] L. M. Sander and T. S. Deisboeck, "Growth patterns of microscopic brain tumors," *Physical Review E: Statistical, Nonlinear, and Soft Matter Physics*, vol. 66, no. 5, Article ID 051901, 2002.

[25] W. G. Tharp, R. Yadav, D. Irimia et al., "Neutrophil chemorepulsion in defined interleukin-8 gradients in vitro and in vivo," *Journal of Leukocyte Biology*, vol. 79, no. 3, pp. 539–554, 2006.

[26] C. W. Frevert, G. Boggy, T. M. Keenan, and A. Folch, "Measurement of cell migration in response to an evolving radial chemokine gradient triggered by a microvalve," *Lab on a Chip*, vol. 6, no. 7, pp. 849–856, 2006.

[27] T. Lämmermann, "In the eye of the neutrophil swarm-navigation signals that bring neutrophils together in inflamed and infected tissues," *Journal of Leukocyte Biology*, vol. 100, no. 1, pp. 55–63, 2016.

[28] S. Kawaguchi and M. Mimura, "Synergistic effect of two inhibitors on one activator in a reaction-diffusion system," *Physical Review E: Statistical, Nonlinear, and Soft Matter Physics*, vol. 77, no. 4, Article ID 046201, 2008.

[29] S. Kawaguchi, "Chemotaxis-growth under the influence of lateral inhibition in a three-component reaction-diffusion system," *Nonlinearity*, vol. 24, no. 4, pp. 1011–1031, 2011.

[30] T. Ohta, M. Mimura, and R. Kobayashi, "Higher-dimensional localized patterns in excitable media," *Physica D: Nonlinear Phenomena*, vol. 34, no. 1-2, pp. 115–144, 1989.

[31] M. Mimura and T. Tsujikawa, "Aggregating pattern dynamics in a chemotaxis model including growth," *Physica A: Statistical Mechanics and its Applications*, vol. 230, no. 3-4, pp. 499–543, 1996.

[32] K. Krischer and A. Mikhailov, "Bifurcation to traveling spots in reaction-diffusion systems," *Physical Review Letters*, vol. 73, no. 23, pp. 3165–3168, 1994.

[33] X.-Y. Chen, "Dynamics of interfaces in reaction diffusion systems," *Hiroshima Mathematical Journal*, vol. 21, no. 1, pp. 47–83, 1991.

[34] P. G. de Gennes and J. Prost, *The Physics of Liquid Crystals*, Oxford University Press, Oxford, UK, 2nd edition, 1995.

[35] L. G. Fel, "Tetrahedral symmetry in nematic liquid crystals," *Physical Review E: Statistical, Nonlinear, and Soft Matter Physics*, vol. 52, no. 1, pp. 702–717, 1995.

[36] H. R. Brand, H. Pleiner, and P. E. Cladis, "Tetrahedratic cross-couplings: Novel physics for banana liquid crystals," *Physica A: Statistical Mechanics and its Applications*, vol. 351, no. 2-4, pp. 189–197, 2005.

[37] T. Hiraiwa, M. Y. Matsuo, T. Ohkuma, T. Ohta, and M. Sano, "Dynamics of a deformable self-propelled domain," *EPL (Europhysics Letters)*, vol. 91, no. 2, Article ID 20001, 2010.

[38] E. Meron, "Pattern formation in excitable media," *Physics Reports*, vol. 218, no. 1, pp. 1–66, 1992.

[39] E. O. Budrene and H. C. Berg, "Complex patterns formed by motile cells of Escherichia coli," *Nature*, vol. 349, no. 6310, pp. 630–633, 1991.

[40] M. Kronlage, J. Song, L. Sorokin et al., "Autocrine purinergic receptor signaling is essential for macrophage chemotaxis," *Science Signaling*, vol. 3, no. 132, p. ra55, 2010.

[41] M. Mimura, H. Sakaguchi, and M. Matsushita, "Reaction-diffusion modelling of bacterial colony patterns," *Physica A: Statistical Mechanics and its Applications*, vol. 282, no. 1, pp. 283–303, 2000.

[42] D. A. Kessler and H. Levine, "Pattern formation in Dictyostelium via the dynamics of cooperative biological entities," *Physical Review E: Statistical, Nonlinear, and Soft Matter Physics*, vol. 48, no. 6, pp. 4801–4804, 1993.

[43] J. Rinzel and D. Terman, "Propagation phenomena in a bistable reaction-diffusion system," *SIAM Journal on Applied Mathematics*, vol. 42, no. 5, pp. 1111–1137, 1982.

[44] I. S. Gradshteyn and I. M. Ryzhik, *Table of Integrals, Series, and Products*, Academic Press, 6th edition, 2000.